SIMULATION OF DYNAMICAL REFRACTIVE INDEX CHANGE IN ON-CHIP
OPTICAL DEVICES

A THESIS SUBMITTED TO
THE GRADUATE SCHOOL OF NATURAL AND APPLIED SCIENCES
OF
MIDDLE EAST TECHNICAL UNIVERSITY

BY

ANIL ASLAN

IN PARTIAL FULFILLMENT OF THE REQUIREMENTS
FOR
THE DEGREE OF MASTER OF SCIENCE
IN
ELECTRICAL AND ELECTRONICS ENGINEERING

SEPTEMBER 2019

Approval of the thesis:

SIMULATION OF DYNAMICAL REFRACTIVE INDEX CHANGE IN ON-CHIP OPTICAL DEVICES

submitted by **ANIL ASLAN** in partial fulfillment of the requirements for the degree of **Master of Science in Electrical and Electronics Engineering Department, Middle East Technical University** by,

Prof. Dr. Halil Kalıpçılar
Dean, Graduate School of **Natural and Applied Sciences**   _____

Prof. Dr. İlkay Ulusoy
Head of Department, **Electrical and Electronics Eng.**   _____

Assist. Prof. Dr. Serdar Kocaman
Supervisor, **Electrical and Electronics Eng., METU**   _____

Examining Committee Members:

Prof. Dr. Mustafa Kuzuoğlu
Electrical and Electronics Engineering, METU   _____

Assist. Prof. Dr. Serdar Kocaman
Electrical and Electronics Eng., METU   _____

Prof. Dr. Barış Bayram
Electrical and Electronics Engineering, METU   _____

Prof. Dr. Hamza Kurt
Electrical and Electronics Engineering, TOBB ETU   _____

Assist. Prof. Dr. Selçuk Yerci
Electrical and Electronics Engineering, METU   _____

Date: 10.09.2019

I hereby declare that all information in this document has been obtained and presented in accordance with academic rules and ethical conduct. I also declare that, as required by these rules and conduct, I have fully cited and referenced all material and results that are not original to this work.

Name, Surname: Anıl ASLAN

Signature:

ABSTRACT

SIMULATION OF DYNAMICAL REFRACTIVE INDEX CHANGE IN ON-CHIP OPTICAL DEVICES

ASLAN, Anıl
Master of Science, Electrical and Electronics Engineering
Supervisor: Assist. Prof. Dr. Serdar Kocaman

September 2019, 72 pages

Theoretical modeling and numerical verification are essential in integrated photonics for designing optimized structures as well as interpretation of the experimental results. In this thesis, a dynamically changing refractive index modification for the Finite Difference Time Domain (FDTD) method is proposed, implemented with C++ and results are compared with recent experimental studies. The proposed method is based on the idea of the time-domain simulation of the non-stationary objects while satisfying the conventional Yee algorithm. As a case study with the proposed modified method, optical analog of the electromagnetically induced transparency (EIT) phenomena in coupled on-chip cavities such as double microring resonators and L3 coupled-cavity photonic crystals is numerically analyzed in detail. Light trapping coming from EIT is an important topic for future photonic integrated circuits and systems observing EIT with micro-cavities are quite suitable for testing dynamical refractive index change. The simulation results with the proposed method are initially verified with an open electromagnetic wave simulator, MEEP, for the constant refractive index cases through the comparison of the transmission spectra. Then, experimental studies are numerically investigated with the proposed modified FDTD method and the calculated delay (light storage) values are consistent with the measurement results proving the usefulness of the developed method.

ÖZ

ÇİP İLE ENTEGRE EDİLMİŞ OPTİK AYGITLARIN DİNAMİK REFRAKTİF İNDİS İLE SİMÜLASYONU

ASLAN, Anıl
Yüksek Lisans, Elektrik ve Elektronik Mühendisliği
Tez Danışmanı: Dr. Öğr. Üyesi Serdar Kocaman

Eylül 2019, 72 sayfa

Teorik gözlemler ve doğrulamalar, fotonik aygıtların deneysel çalışmaları için önemlidir. Bu tezde, çift yüzük rezonatörler ile L3 boşluk eşlenik fotonik kristallerin, C++ ile kodlanmış dinamik sınırlı değişkenli zaman eksenli metot ile simüle edilmesi gerçekleşmiştir ve bu simülasyon sonuçları deneysel çalışmalarla kıyaslanmıştır. C++ ile kodlanmış bu metodun amacı, Yee algoritmasına bağlı kalınarak dinamik yapıların zamanda simülasyonudur. Elektromanyetik indüklenme geçirgenliği ile de çift yüzük rezonatörler ile L3 boşluk eşlenik fotonik kristallerin numerik simülasyonları gerçekleşmiştir. Işığın elektromanyetik indüklenme geçirgenliği ile depolanması yeni nesil fotonik aygıtlar için önemli olan bu konu dinamik refraktif indis değişkenliğini test ve doğrulanması için uygundur. Öne sürülen bu metodun simülasyon sonuçları açık kaynak kodlu araç olan MEEP ile sabit refraktif indis ile karşılaştırılmıştır. Ayrıca deneysel çalışmalar bu metot ile de incelenmiş ve ışığın zamandaki kayması doğrultusunda depolanması gözlemlenmiştir.

Anahtar Kelimeler: dinamik sınırlı değişkenli zaman çizelgesi metodu, hesaplamalı elektromanyetik, yüzük rezonatörler, fotonik kristaller

To my family

ACKNOWLEDGEMENTS

TABLE OF CONTENTS

LIST OF FIGURES

FIGURES

xiv

LIST OF ABBREVIATIONS

ABBREVIATIONS

PCB   Printed Circuit Board

MOS   Metal Oxide Semiconductor

SiPh   Silicon Photonics

EM   Electromagnetic

EIT   Electromagnetically Induced transparency

PhC   Photonic Crystals

FDTD   Finite Difference Time Domain

GMT   Generalized Multipole Technique

MMP   Multiple Multipole Technique

FMM   Fourier Modal Method

FVTD   Finite Volume Time Domain Method

PSTD   Pseudospectral Time Domain

FDFD   Finite Difference Frequency Domain

FEM   Finite Element Method

DGTD   Discontinuous Galerkin Time Domain

ABC   Absorbing Boundary Condition

TFSF   Total Field/Scattered Field

WDM   Wavelength Division Multiplexing

EMF   Electromotive force

LIST OF SYMBOLS

SYMBOLS

Λ Resonant wavelength of a ring resonator

r Radius

a Lattice period

w   Cavity resonance frequency

τ Photon lifetime

t   Time

Q   Quality factor

Δ_t Temporal step

Δ_x Spatial step

S_c Courant number

m/s Meter per second

ms   Millisecond

ps   Picosecond

$\vec{B}$ Magnetic flux density

$\vec{H}$ Magnetic field

$\vec{D}$ Electric flux density

$\vec{E}$ Electric field

$\vec{J}$ Electric current density

ρ_V	Charge on volume
Φ	Magnetic flux
V	Volume
∇	Cross Product
I_{enc}	Enclosed Current
δ	Approximation error
ϵ_0	Permittivity
μ_0	Permeability
m	Sampling ratio of spatial step
q	Sampling ratio of time step
c	Speed of light
σ	Conductivity
P	Power intensity
ϕ	Phase angle
k	Cross-coupling coefficient
r	Self-coupling coefficient
H_{21}	Coupling-matrix element
$\vec{T}_{d\hat{z}}$	Translational Symmetry
n	Band number
θ	Incident angle
n_{eff}	Effective index

d   The distance between rows of PhC

$\vec{R}$ Rotational Symmetry

L_{12} Separation distance between cavities 1 and 2

κ Coupling Equation

CHAPTER 1

INTRODUCTION

1.1. Objectives

The light manipulation is a trending research topic in optical devices. Many researches aim to reflect, store, or propagate light inside the silicon-based artificial optical devices. These works depend on the improvement of communications among continents, builds or printed circuit boards [1-9]. Under certain conditions, manipulation of light could be useful and efficient more than conventional electronics. The limitations of the conventional electronics, analog metal-oxide semiconductors (MOS) devices, force the border of the silicon. Therefore, the works for light manipulation widen the conventional MOS devices [10]. The silicon photonics (SiPh) becomes the hybrid area of both silicon device and light manipulation worlds. Therefore, the availability and cost-efficiency of the silicon devices provide the rapid and reliability of light manipulation, and the hybrid optical devices offer advantageous solutions.

Ring resonators and photonic crystals (PhC) are two applications in the photonics area. These devices are artificially composed of silicon. Their principle is based coupling of the light inside the devices. Therefore, filtering, propagation, and store of light could be possible [11,12,13]. Ring resonators filter the light regarding wavelength, which is like an add-drop filtering. PhCs propagate the light along the cavities inside a structure. In this thesis, to perform the simulations, the modified version of a ring resonator and PhC provide a dynamical tuning of the light. This ability offers that the light is possible to be stored inside a structure depending on the lifetime of the resonances.

The electro-optical properties of the silicon make it possible to trap the light and propagate alongside the structure [6,7]. Therefore, the resulted structures provide a

tuning mechanism of light with coupling in an efficient way. The light manipulation depends on the electromagnetically induced transparency (EIT) phenomena [14,15]. The phenomena exist while the material properties no longer be affected. It is a technique for the elimination of the medium. The interaction of electrons with the light changes the optical response of the atoms [16]. The basis of the EIT is the opposite movement of the electrons which interfere with each other. Therefore, electrons cannot move anymore, which means that the medium creates a window for transparency. This phenomenon can be observed at not only photonics but also mechanical systems, basic RLC circuits, atomic states or plasmonic systems [16]. In optical devices, EIT provides a light trap or store. Therefore, using this transparency, the ultraslow light propagation [2], light storage [5], dissipation-free light transmission [4] and nonlinear optics with light propagation can be applied.

Analyzing the EIT concept, the system consists of two spring can be illustrated. The mechanical system behaves like a three-level atomic states. The springs oscillate harmonically depending on their spring constants. If the power absorbed from one of the materials, the EIT case can be observed by measuring the power absorption from the masses. The case for identical mass and constants results in an identical power absorption. However, a little change in the spring constants changes the behavior of the springs and create transparency in an absorbed power. At that oscillation frequency, no power is absorbed from the masses. The RLC circuit is another system for an observation of the EIT. In the case of the RLC circuits, the L and C components determine the resonance frequencies. The switch inside the RLC circuit is the tuning factor for the EIT case. Again, by measuring the power which is transferred from the voltage source, the EIT case can be observed. The switch creates a detuning with resonance frequencies of the LC components. Therefore, the little difference in the frequencies results in an EIT case which does not have power transfer from the voltage source [53].

For the optical systems, this phenomenon can be used to trap the light inside a structure which are experimentally demonstrated [6,7,8,9]. These experiments create a transparency window by again detuning resonance frequencies which are based on medium behaviors. Then, by manipulating the medium, which will be explained in the following chapters, the transmission results in a peak at the deep. The light manipulation is used for the light trapping inside a structure. In this thesis, the double microring resonator and L3 coupled-cavity PhC structures will be analyzed and simulated by using the EIT.

Optical devices have many advantages with using manipulation of light. The experiments have results with many applications such as light trapping, waveguide division multiplexing (WDM), waveguide splitter, waveguide crossings. However, the simulation of the optical devices is compulsory for the optimum results. Performing EM analysis of the optical devices, the conversion of electromagnetic (EM) waves into the computational word is needed. The major method of conversion is discretization. It should be taken that the discretization compromises the propagation of light under certain conditions. The propagation can be obtained with iteration of the EM equations [17]. To obtain correct analysis of EM, discretization forces to put the EM waves into closed numerical forms. The stored discrete values should be obtained because of the set of equations in limits. One of the primary methods, obtaining the numeric solutions for computational world is the Finite Difference Time Domain (FDTD). The method provides approximate solutions in a discrete form. The method is based on the discrete forms of iterated values in a finite-difference. In other words, EM waves can be discretized with FDTD and iterated on a time scale. Therefore, FDTD is an essential method for numerical analysis and the basis of the simulation tools for optical devices [18].

The FDTD is a flexible method to adapt against many circumstances, such that size, material selection, boundaries, electro-optical effects, etc. It can be said that the method can be applied to various types of optical devices. The arrangements of the experimental environments provide correct estimated values of the EM waves concerning light

manipulation inside a structure. Once the stable conditions are illustrated, the method iterates the EM waves in an order. However, the main challenge here is the simulation of the non-stationary objects. The method can be improved for the optical devices which are moving, altering, or shifting. The necessity of the non-stationary object simulation results in a dynamic FDTD method. This improved method increases the flexibility of the FDTD method regarding of non-stationary objects. During the simulation, in a finite difference, the object or environment can be modified, and EM waves can continue to iterate on a time scale. Therefore, the dynamic FDTD method raises the certainty of the simulation concerning vivid experimental conditions.

In this thesis, the C++ coded dynamic FDTD method is proposed. This method can simulate the non-stationary objects on a time scale. Here, the proposed method focusses on the refractive index change of the photonic devices such as double microring resonator and L3 coupled-cavity PhC. These structures have experiments which demonstrate the light trapping with a dynamic tune of the refractive index of the structures. Therefore, light trapping is simulated with the proposed method under dynamical behaviors.

1.2. Literature Survey of Computational EM

The Computational EM regarding of the FDTD method is firstly illustrated by Kane Lee [19]. He proposed the iteration of waves that are deducing from Maxwell's equations which are given in detail in chapter 2. Beyond the FDTD method, there are other methods to evaluate EM waves. The generalized multipole technique (GMT) is one of the methods to analyze EM waves. This method provides a simulation of multipole spherical objects [20]. The observations of the electromagnetically scatterings are available by the GMT uses the origins of the spherical objects. Also, its developed version is called a multiple multipole technique (MMP) which is multiple point matches inside the spherical objects to increase the accuracy of the GMT [21].

The photonic Wannier function is another method for electromagnetically simulation of PhC. The Wannier function can be used as a set of photonic band gaps modeling [21,23]. Then, the functions are available to analyze the properties of the PhC. However, the method is the lack of time-domain analyses.

Fourier modal method (FMM) is used to simulate layered periodic structures. From the Rayleigh solutions, the FMM deduces the homogenous solutions of the EM fields [24,25,26]. Then, these solutions are analyzed with S-matrix approaches of the linear system. The main issue about the methods, GMT, MMP, Wannier function, and FMM is that they are case-specific simulation methods. Beyond their specific cases, the methods need a few information to infer the EM fields. This idea means that they are relatively less flexible than other methods for EM simulation.

The finite volume time domain method (FVTD) is another method to simulate the EM wave by slicing the EM fields into small volumes [27,28]. It uses the boundary conditions of the EM fields to calculate the next step of the fields. The method has the advantage to simulate irregular structures, but it needs to define the structure grids that are a complicated step to simulate EM waves.

The pseudospectral time domain (PSTD) is the method to give the approximation simulation of EM fields. This method takes the Fourier transform of the spatial steps for derivation. Then the inverse Fourier transform is held to get back the spatial domain [29, 30]. Since there is multiple transformation, the numerical dispersion rises. So, the stability criterion is much more limited to arrange during the time domain simulation. Therefore, the flexibility reduces.

Another method based on frequency domain analyses is the finite difference frequency domain (FDFD). This method provides flexibility in the steady-state solutions of simulation of the EM fields [18]. In a frequency domain, the spectral analyses of EM

5

fields at a specific frequency can be easily simulated by FDFD. However, the method suffers from the time domain responses of the large devices. Also, the response along the time slots can be harsh with the FDFD methods.

The finite element method (FEM) is one of the conventional methods to simulate EM fields [18,30-32]. Like the FVTD, the method slices the space into small pieces. Therefore, the complex geometrical structures can be easily simulated by FEM. Also, the random distribution of each piece is arranged simply by this method. However, the time response could be complicated for FEM since into each finite element, the system of linear equations should be taken. Therefore, this issue increases the computational cost. Then, the discontinuous Galerkin time domain (DGTD) method is introduced to overcome the time issue [33]. The DGTD aims to combine FEM and FDTD methods. It is said that the DGTS can provide both time response of the structure and the spectral analysis in a small piece. Thus, the DGTD needs more information about the interface points of the EM fields. Therefore, it can be said that DGTD requires more computation to simulate the EM fields at initialization [34].

Thus far, the other methods for EM analyses are explained. However, in this thesis, we focused on the FDTD method which has considerable advantages [18]. The method eases simulation to create the numerical grid. Also, it can be available for discretization by just interpreting Maxwell's equation in a discrete form. Also, it provides the EM simulation in the time domain.

Although the FDTD method has significant features, there is a drawback which is that the method is just used for stationary objects. To overcome this issue, Q. Jiang found a way to simulate moving 2D PhC by the FDTD method [35]. He experimentally observed the behavior of the inverse Doppler Effect in 2D PhC on phase evolution. Then, he simulated the light, which is transmitting through the moving PhC. So he provided a comparison of the theoretical and experimental results. He proposed a dynamical form of the FDTD method. This method provides the movement of PhC varied by manipulating the dielectric constant and magnetic permeability at each

temporal step. Then, he developed an improvement in the FDTD method at the time step at which the EM fields are following each other. He also proposed that a small-time step duration limits the dynamic movement of the 2D PhC.

Since Q. Jiang proposed the improved version of the FDTD method, the EM fields can be simulated in motion on a time scale. However, in this improvement, the motion is the only dynamic factor. In this thesis, the C++ coded FDTD method is a proposed method which can simulate dynamic refractive index change of the structure on a time scale. Therefore, the medium can alter its behavior concerning refractive index variations. Moreover, the light trapping issue based on medium change can be simulated under the dynamical behavior of structures. By following this idea, in the next chapters, the double microring resonators and L3 coupled cavity PhC are analyzed and simulated with the proposed FDTD method.

1.3. The Researches About The Light Trapping

To store or slow the light inside a structure is demonstrated in many other ways. L. V. Hau experimentally observed that light propagates at 20 million times slower in an ultracold gas of sodium atoms than air [2]. The atoms were cooled at nanokelvin temperatures by laser. Then the light speeds reduced at 17 m/s.

At room temperature, M. S. Bigelow lowered the speed of the light at 91 m/s in alexandrite crystal [1]. The crystal is composed of different states of ions. At the inversion state, ions have longer relaxation time around 50 ms. Therefore, excited electrons are limited, and light is slower.

S. Ghosh showed that the light interacts with the use of acetylene in an HC-PBF fiber [3]. The interactions create a transparency window which means EIT. And the light is delayed around 800 ps inside an HC-PBF.

C. Liu achieved light stopping around 1 ms. He put the light inside a cold cloud of sodium atoms and created a magnetic trap. Rapid turn-off of coupling laser results in

a sudden stop of the light [4]. Then the laser is turned on again. He concluded that this tuning provides read and write functions.

Double microring resonator is experimentally observed by M. Lipson, Q. Xu, and their research group. They investigated the light with its delay-bandwidth limits [6,7] and trapped the light inside a resonator with a 1.5ps control pulse which caused a blue-shift effect. Therefore, the effect differed from the refractive index of one of the rings that uncoupled with waveguide. Then, the light continuously propagated alongside the resonator during the 700 ps lifetime. So, they dynamically tuned the structure to release the light and detuned for trap again. As a result, they obtained a fast electrooptic tuned resonator. Also, their other work provided the EIT concept of the double microring resonator [6]. In this work, they proposed that a difference between rings still provides a trap of the light inside a resonator and EIT phenomena. He compared the results concerning various diameters of the ring.

Photonic crystals are artificial structures. They can compose waveguides, step-index fiber, grading coupler. Here, L3 cavity Photonics Crystals are simulated. The L3 cavity PhC is experimental demonstrated by X. Yang and S. Kocaman [8,9]. They used the same structure, but S. Kocaman provided group delays with the tune – detune cases. X. Yang compared the various results of the EIT case concerning the wavelength difference. He eventually showed the case that the EIT no longer exists. S. Kocaman resulted in multiple tune cases. He experimentally showed that the light traps inside the cavities between the tune-detune period on a time scale.

The last two experimental studies, the double microring resonator, and the L3 coupled cavity PhC are the focus of the thesis. The rest of the thesis, these photonic devices will be analyzed since they are applicable to be simulated with the proposed FDTD method. These studies base on the refractive index change of the structure for the dynamic tuning. Therefore, the proposed method can simulate these structures with both conventional and dynamical forms.

1.4. Outline of The Thesis

This thesis focuses on the computational analysis of the double microring resonator and L3 coupled cavity PhC with a dynamic FDTD method.

The following chapter will be the explanation of the EM wave theory with analyzing Maxwell's equations. The discrete forms of Maxwell's equation will be studied to reach the iteration form of the computational FDTD method. Then, the FDTD method interpretation will be inferred from the derivative and integration form of the discrete Maxwell's equations. Also, the computational form of the FDTD and its improvements for the experimental circumstances will be discussed. Modifications to the conventional form of the FDTD method will explain the proposed FDTD method. The dynamic approach of the FDTD method will be discussed to form the simulation of the active structures by change of the effective refractive index of the optical devices.

The third chapter is about the ring resonators. The various types of ring resonators will be given with their theoretical explanations. Then, the double microring resonator will be given with its serial and parallel connected models. The verification of the proposed method on a double microring resonator, the experimental study about the dynamical tuning will be simulated with both conventional and the proposed FDTD individually. Later, these cases will be used to compare the simulation results of both the proposed FDTD method and the conventional FDTD tool, MEEP. The experimental results will also be used to verify the simulation of detuning od the structure with observations of delay cases of the incident light source.

The fourth chapter mentions the PhC and its underlying principles for the coupling of light. The various types of PhC will be explained to analyze the crystal structure. Then, the L3 cavity coupling PhC will be again analyzed with comparative results with conventional FDTD and the proposed dynamic FDTD. The spectral analysis and transmission results of the resonant cavities are also given. So, the delay of the light because of light trapping is observed during the propagation of the light inside the

PhC. To verify the proposed method on the structure, the experimental study about the detuning of the L3 coupled cavities will be examined with both conventional and dynamical FDTD individually. Later, these cases will be used to compare the simulation results of both the proposed FDTD method and the conventional FDTD tool, MEEP. The experimental results will also be used to verify the simulation of detuning od the structure with observations of delay cases of the incident light source.

The last chapter is the conclusion and discussions. There would be a summarize of the thesis topic. Also, future developments section is given to explain improvements about the proposed dynamic FDTD method. In the end, the references section will follow.

CHAPTER 2

THE INTERPRETATION OF THE PROPOSED FINITE DIFFERENCE TIME DOMAIN METHOD

2.1. EM Wave Theory

The propagation of light inside an electromagnetic medium represents the set of Maxwell's equations [11, 29, 36]. They have four equations for propagation, interaction, and influence of electric and magnetic fields. These equations are,

$$\nabla . \vec{D} = \rho_V \tag{2.1}$$

$$\nabla . \vec{B} = 0 \tag{2.2}$$

$$\nabla \times \vec{E} = -\frac{\partial \vec{B}}{\partial t} \tag{2.3}$$

$$\nabla \times \vec{H} = \frac{\partial \vec{D}}{\partial t} + \vec{J} \tag{2.4}$$

These four equations state that electric and magnetic fields have related to each other. The current flow results in a magnetic field. So, the divergence of the current concerning time makes the magnetic field arises in the electric field. It also charges both positive and negative increases in electric field density [18, 19], and the further increase results in magnetic field propagation. Each equation has a specific meaning. Equation 2.1 and 2.2 are called Gauss' Law. Equation 2.3 is referred to as Faraday's Law and Equation 2.4 is Ampere's law [17].

Gauss' law states conservation of charges is the initialization of the electric field [37]. This conservation can be observed by integrating Equation 2.1.

$$\int (\nabla . \vec{D}) dV = \int \rho_V \, dV \qquad (2.5)$$

$$\int \vec{D} ds = Q_{enc} \qquad (2.6)$$

Then, it is observed with Equation 2.6. This total charge is depending on the total electric field over the surface. Further interpretation can be proposed as the electric field is caused by electric charges [29, 36].

Gauss' 2nd Law, Equation 2.2, states that there is no magnetic charge. The divergence of B fields should be zero all the time. This result means that there are no magnetic monopoles to create magnetic fields. The magnetic fields should flow over a closed-loop [38].

Equation 2.3 is the Faraday's Law which says that divergence of magnetic flux over time creates an electric field and indeed, an electric current or vice versa. This thought depends on the Lens' laws which is [27],

$$EMF = -\frac{d\Phi}{dt} \qquad (2.7)$$

This equation means that magnetic flux creates an electromotive force which is a basic voltage source. Then, the voltage is defined as,

$$\int \vec{E} dl = V \qquad (2.8)$$

So, EMF is related to the electric field as,

$$\int \vec{E} dl = EMF \qquad (2.9)$$

Using a Stokes' theorem, which states that integration over the field is equal to integrating the curl of the field over a loop. By modifying Equation 2.8 [17],

$$\int \vec{E}\, dl \;=\; \int \nabla x \vec{E}\; ds \qquad\qquad (2.10)$$

which results in $\nabla \times \vec{E} = -\dfrac{\partial \vec{B}}{\partial t}$ as in Equation 2.3.

Then, Faraday's Law states that electric and magnetic fields are related inversely. Time dependence change creates an electric field and, electrical curl creates a magnetic field.

Ampere's Law is given as Maxwell's 4th equation which is the consequence of the electric current which is equal to the integration of the magnetic field as in Equation 2.11 [29, 37].

$$\int \vec{H}\, dl \;=\; I_{enc} \qquad\qquad (2.11)$$

which states that any current through the line produces a magnetic field around it. If Equation 2.11 is manipulated using Stokes' theorem as [17, 18, 19],

$$I_{enc} \;=\; \int \vec{H}\, dl \;=\; \int \nabla x \vec{H}\; ds \qquad\qquad (2.12)$$

Also, it is known that current can be defined as,

$$\int \vec{J}\, dS \;=\; I_{enc} \qquad\qquad (2.13)$$

As a result, with combining Equations 2.12 and 2.13,

$$\int \vec{J}\, dS \;=\; \int \nabla x \vec{H}\; ds \qquad\qquad (2.14)$$

$$\nabla x \vec{H} = \vec{J} \qquad\qquad (2.15)$$

However, mathematically it should be satisfied that divergence of the curl should be zero. Equation 2.15 satisfies the condition when the divergence of the $\vec{J}$ is zero. This has a possibility, but it cannot be generalized [17, 18, 19]. Therefore, based on the opposite idea of the magnetic field creates an electric field, electric field density can

produce current density with charge displacement. Then, it is found that displacement current density is the time-varying derivation of the electric field density [29, 37, 46]. Then, Equation 2.15 becomes,

$$\nabla x \vec{H} = \vec{J} + \vec{J_D} \tag{2.16}$$

$$\nabla x \vec{H} = \vec{J} + \frac{\partial \vec{D}}{\partial t} \tag{2.4}$$

Maxwell's equations are the basis of the EM wave analysis. Since the dependence between the electric field and magnetic field, these fields can be interpreted from each other. The focus here is the interpretation of the fields. Fields are continuous and affected each other. However, for the computational world, these equations should be converted into the discretized closed forms [17, 19, 29]. Therefore, in the following section, the FDTD method and discretized forms will be discussed.

2.2. The Interpretation of the Finite Difference Time Domain Method

The Finite Difference Time Domain Method gives results of approximation of the EM fields. The basis of the method is based on Taylor series expansion which is the approximation of derivation. By combining both Taylor's expansion with Maxwell's equations, the FDTD method can be interpreted [17,29]. Taylor series expansion of function $f(x)$ is defined around x_0 with an error of $\pm \frac{\delta}{2}$ as,

$$f\left(x_0 + \frac{\delta}{2}\right) = f(x_0) + \frac{\delta}{2} f'(x_0) + \frac{1}{2!}\left(\frac{\delta}{2}\right)^2 f''(x_0) + \frac{1}{3!}\left(\frac{\delta}{2}\right)^3 f'''(x_0) + \cdots \tag{2.17}$$

$$f\left(x_0 - \frac{\delta}{2}\right) = f(x_0) - \frac{\delta}{2} f'(x_0) - \frac{1}{2!}\left(\frac{\delta}{2}\right)^2 f''(x_0) - \frac{1}{3!}\left(\frac{\delta}{2}\right)^3 f'''(x_0) - \cdots \tag{2.18}$$

Subtracting Equations 2.17 and 2.18 yields,

$$f\left(x_0 + \frac{\delta}{2}\right) - f\left(x_0 - \frac{\delta}{2}\right) = \delta f'(x_0) + \frac{2}{3!}\left(\frac{\delta}{2}\right)^3 f'''(x_0) + \cdots \tag{2.19}$$

After manipulation,

14

$$\frac{\left(f\left(x_0 + \frac{\delta}{2}\right) - f\left(x_0 - \frac{\delta}{2}\right)\right)}{\delta} = f'(x_0)\frac{1}{3!}\left(\frac{\delta}{2}\right)^2 f'''(x_0) + \cdots \tag{2.20}$$

The left-hand of the equality indicates the derivative of the $f(x)$ at x_0. So, the right-hand side of Equation states a function depends on δ^2. If Equation 2.20 is rearranged as [17, 29, 36],

$$\left.\frac{df(x)}{dx}\right|_{x=x_0} = \frac{f\left(x_0 + \frac{\delta}{2}\right) - f\left(x_0 - \frac{\delta}{2}\right)}{\delta} + F(\delta^2) \tag{2.21}$$

Equation 2.21 can be approximated as follows. It is known that δ^2 term is so small. So if Equation 2.20 is advanced, there would be δ^4, δ^6, δ^8, ... terms. Regarding small δ, these terms can be neglected [17, 18, 37]. Indeed, in Equation 2.21, $F(\delta^2)$ can be neglected too. Therefore, the approximated form of Equation 2.21 becomes,

$$\left.\frac{df(x)}{dx}\right|_{x=x_0} \approx \frac{f\left(x_0 + \frac{\delta}{2}\right) - f\left(x_0 - \frac{\delta}{2}\right)}{\delta} \tag{2.22}$$

This equation becomes the central difference which equals the derivation of function around small δ. This approximation is second-order behavior. There is an error in this approach due to the value of δ. If the δ becomes zero, then the approximation gives a correct result without error [18, 29, 37]. The approximation in Equation 2.22 improves the field iteration of the FDTD method.

Kane Yee firstly demonstrated the FDTD method in 1960. He stated the algorithm for the FDTD as using second-order central differences [19]. According to him, the FDTD method is a complete set of derivative forms of Maxwell's equations. As a result of the approximated behavior of Equations, the electric and magnetic fields are obtained with updated forms of discrete equations. For the advance values of the EM fields, the time scale second-order central difference is used the former values of EM fields [17, 29, 36]. Each time step, this algorithm is followed in order. To establish the multi-dimensional form of the FDTD, initially 1D form is constructed.

Consider the 1D space that the electric field only has a z component. So in a linear medium, regarding of Maxwell's equations, the fields become as [18, 19, 26, 37],

$$-\frac{\partial \vec{B}}{\partial t} = -\mu \frac{\partial \vec{H}}{\partial t} = \nabla \times \vec{E} = -\hat{a}_y \frac{\partial E_z}{\partial x} \qquad (2.23)$$

$$\frac{\partial \vec{E}}{\partial t} = \epsilon \frac{\partial \vec{D}}{\partial t} = \nabla \times \vec{H} = \hat{a}_z \frac{\partial H_y}{\partial x} \qquad (2.24)$$

Then, in scalar forms of Equations become,

$$\mu \frac{\partial H_y}{\partial t} = \frac{\partial E_z}{\partial x} \qquad (2.25)$$

$$\epsilon \frac{\partial E_z}{\partial t} = \frac{\partial H_y}{\partial x} \qquad (2.26)$$

From Equations 2.25 and 2.26, it can be interpreted that an electric field can be calculated from the magnetic field. So, the advance values of the magnetic field can be calculated from the former electric field. Therefore, the fields can be calculated from the former values on a continuous scale.

If these equations are adapted regarding of the computational world, Equations become discrete. To have discrete values of fields, the time and the space should be in the form of discrete values. Therefore, each space and time should be sampled with a ratio of m in space and with a ratio of q in time. Therefore, with a small Δ_x and Δ_t, $x = m\Delta_x$, and $t = q\Delta_t$[17, 18, 29].

$$E_z(x, t) = E_z(m\Delta_x, q\Delta_t) = E_z^q[m] \qquad (2.27)$$

$$H_y(x, t) = H_y(m\Delta_x, q\Delta_t) = H_y^q[m] \qquad (2.28)$$

1D Yee Cell is shown in the Fig 2.1, which is redrawn by MATLAB [17.19]. The cell is in both space and time. It consists of E_z and H_y fields in a discrete form. Regarding past times, the Yee grid can be illustrated using approximated the FDTD method as in Equations 2.27 and 2.28.
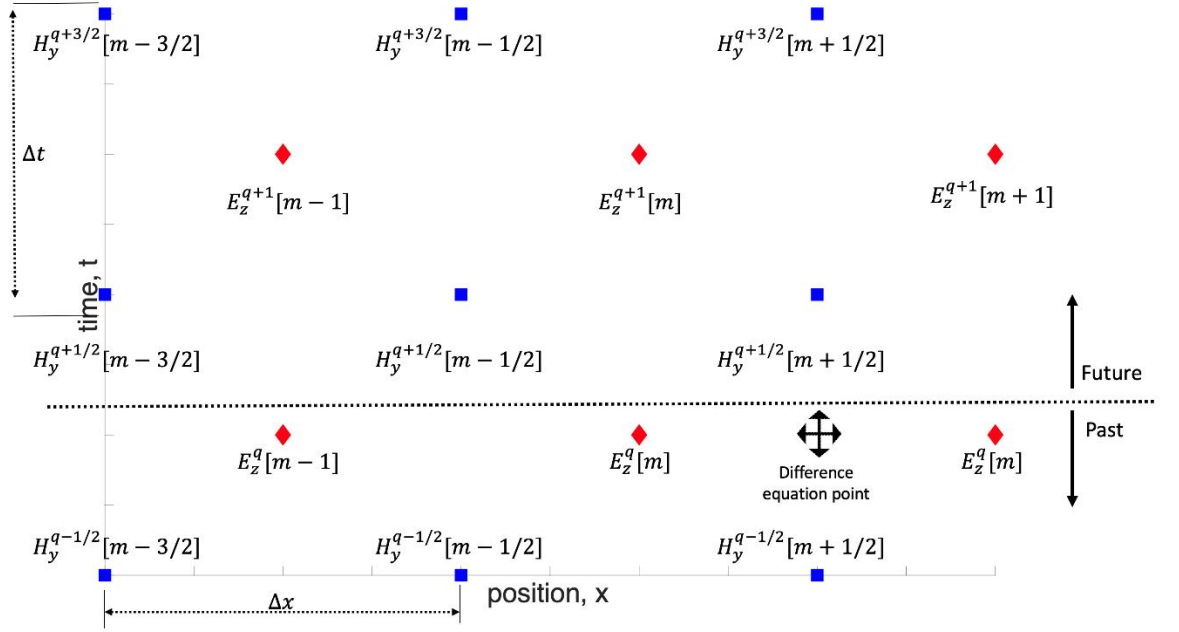

$H_y^{q+3/2}[m-3/2]$ $H_y^{q+3/2}[m-1/2]$ $H_y^{q+3/2}[m+1/2]$

Δt

$E_z^{q+1}[m-1]$ $E_z^{q+1}[m]$ $E_z^{q+1}[m+1]$

time, t

$H_y^{q+1/2}[m-3/2]$ $H_y^{q+1/2}[m-1/2]$ $H_y^{q+1/2}[m+1/2]$ Future

Past

$E_z^q[m-1]$ $E_z^q[m]$ Difference equation point $E_z^q[m]$

$H_y^{q-1/2}[m-3/2]$ $H_y^{q-1/2}[m-1/2]$ $H_y^{q-1/2}[m+1/2]$

Δx position, x

Figure 2.1. The Yee Cell in Discrete Form and Update Equation for Hy[17]

According to Fig 2.1, the discrete equation can be derived at the point $\left(m+\frac{1}{2}\right)\Delta_x, q\Delta_t$ as follows [17, 18 37],

$$\mu\left.\frac{\partial H_y}{\partial t}\right|_{\left(m+\frac{1}{2}\right)\Delta_x,q\Delta_t} = \left.\frac{\partial E_z}{\partial x}\right|_{\left(m+\frac{1}{2}\right)\Delta_x,q\Delta_t} \qquad (2.29)$$

17

Equations 2.29 can be approximated as Taylor series expansion as in Equations 2.22 below.

$$\mu \, \frac{H_y^{q+\frac{1}{2}}\left[m+\frac{1}{2}\right] - H_y^{q-\frac{1}{2}}\left[m+\frac{1}{2}\right]}{\Delta_t} = \frac{E_z^q[m+1] - E_z^q[m]}{\Delta_x} \quad (2.30)$$

In the FDTD form, Equation 2.30 becomes [17, 18, 37],

$$H_y^{q+\frac{1}{2}}\left[m+\frac{1}{2}\right] = H_y^{q-\frac{1}{2}}\left[m+\frac{1}{2}\right] + \frac{\Delta_t}{\mu\Delta_x}\left(E_z^q[m+1] - E_z^q[m]\right) \quad (2.31)$$

Then, Equation 2.31 yields the update equation for H_y. This equation would be used for obtaining future values of the magnetic field with adjacent electric fields at time q.
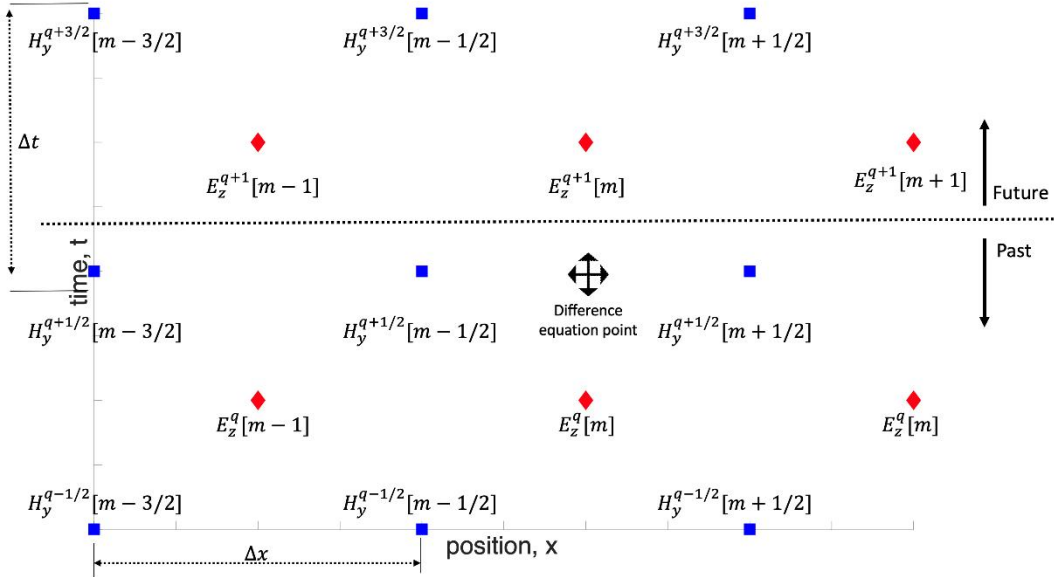

Figure 2.2. The Yee Cell in Discrete Form and Update Equation for Ez[17]

18

Now, it should be indicated that the electric field could be discretized for its future values. Therefore, as in the Fig 2.2, which is redrawn by MATLAB [17,19], Maxwell's equations are rearranged.

According to Fig 2.2, the discrete equation can be derived at the point $m\Delta_x, (q + \frac{1}{2})\Delta_t$ as follows,

$$\epsilon \left. \frac{\partial E_z}{\partial t} \right|_{m\Delta_x,(q+\frac{1}{2})\Delta_t} = \left. \frac{\partial H_y}{\partial x} \right|_{m\Delta_x,(q+\frac{1}{2})\Delta_t} \tag{2.32}$$

Equations 2.32 can be approximated as Taylor series expansion as in Equations 2.22 below [17, 18, 37].

$$\epsilon \frac{E_z^{q+1}[m] - E_z^q[m]}{\Delta_t} = \frac{H_y^{q+\frac{1}{2}}\left[m + \frac{1}{2}\right] - H_y^{q+\frac{1}{2}}\left[m - \frac{1}{2}\right]}{\Delta_x} \tag{2.33}$$

In the FDTD form, Equation 2.31 becomes,

$$E_z^{q+1}[m] = E_z^q[m] + \frac{\Delta_t}{\epsilon \Delta_x}\left(H_y^{q+\frac{1}{2}}\left[m + \frac{1}{2}\right] - H_y^{q+\frac{1}{2}}\left[m - \frac{1}{2}\right]\right) \tag{2.34}$$

Thus, Equation 2.34 yields an update equation form of E_z. This equation means that as the procedure to find H_y, E_z can be found with using the magnetic fields from the past values of the E_z and close H_y fields.

Equations 2.30 and 2.34 have coefficients, $\frac{\Delta_t}{\mu\Delta_x}$ and $\frac{\Delta_t}{\epsilon \Delta_x}$ respectively. These coefficients can be represented by using the speed of light in free space as [17, 18, 37].,

$$c = \frac{1}{\sqrt{\mu_0 \epsilon_0}} \tag{2.35}$$

It can be said that the maximum available energy in a spatial grid is $c\Delta_t$. Therefore, for the stability issues, the ratio of $\frac{c\Delta_t}{\Delta_x}$ is called a Courant number, labeled S_c[18, 29, 37]. With using the S_c the coefficients in Equations 2.31 and 2.34 can be rearranged.

As a result, the FDTD method forms can be operated under stability limits. In a linear medium, $\mu = \mu_r \mu_0$ and $\epsilon = \epsilon_r \epsilon_0$. Let define $\eta_0 = \sqrt{\frac{\mu_0}{\epsilon_0}}$ Then, the coefficients become [18, 29, 37],

$$\frac{\Delta_t}{\mu \Delta_x} = \frac{1}{\mu_r \mu_0} \frac{\sqrt{\mu_0 \epsilon_0}}{\sqrt{\mu_0 \epsilon_0}} \frac{\Delta_t}{\Delta_x} = \frac{\sqrt{\mu_0 \epsilon_0}}{\mu_0 \epsilon_0} \frac{c \Delta_t}{\Delta_x} = \frac{1}{\mu_r} \sqrt{\frac{\epsilon_0}{\mu_0}} \frac{c \Delta_t}{\Delta_x} = \frac{1}{\eta_0 \mu_r} \frac{c \Delta_t}{\Delta_x} = \frac{1}{\eta_0 \mu_r} S_c \quad (2.36)$$

$$\frac{\Delta_t}{\epsilon \Delta_x} = \frac{1}{\epsilon_r \epsilon_0} \frac{\sqrt{\mu_0 \epsilon_0}}{\sqrt{\mu_0 \epsilon_0}} \frac{\Delta_t}{\Delta_x} = \frac{\sqrt{\mu_0 \epsilon_0}}{\mu_0 \epsilon_0} \frac{c \Delta_t}{\Delta_x} = \frac{1}{\epsilon_r} \sqrt{\frac{\mu_0}{\epsilon_0}} \frac{c \Delta_t}{\Delta_x} = \frac{\eta_0}{\epsilon_r} \frac{c \Delta_t}{\Delta_x} = \frac{\eta_0}{\epsilon_r} S_c \quad (2.37)$$

Considering the stability issues of the FDTD method, the propagation can rapidly give tremendous results when the time step is taken too large. Therefore, courant number S_c, provides reasonable values for the FDTD method. The method has an algorithm to find EM fields using both past values and close EM fields. Therefore, the method is affected only for one Δ_x [17, 18, 29, 37]. This effect means that the energy the maximum energy providing in a spatial step can be restricted with the inequality as in Equations 2.38.

$$c \Delta_t \leq \Delta_x \quad (2.38)$$

is satisfied, when the maximum energy providing in a spatial step is limited with Δ_x. As a result, the courant number S_c is limited as $S_c \leq 1$ [17,29].

The 1D analytical results are reasonable for the computational world. For the simulation, these discrete forms of the Maxwell equations can be used to propagate light with an analysis of EM waves. However, conversion of the Maxwell's equations into discrete form is not enough for simulation of the optical devices. Since there exist a few limited and vivid factors, the methods could be improved to illustrate realistic conditions more efficient way.

2.3. The Computational Analysis of The Proposed FDTD Method

The FDTD method is a discrete form of Maxwell's equations. It is an efficient way to analyze the EM waves in a time scale. Since the FDTD method is composed of grids, each grid should be specified in an allocated memory [17, 18]. The past forms of the EM waves are used for the advance values of the EM waves. Because of the time domain, each time cycle, the FDTD method is repeated. Thus, there should be a memory, allocated for recording EM waves.

Then, the structure and its material properties are defined for the propagation of the light and boundaries of the EM waves. This definition is completed at the beginning of the computational analysis. The basic form of the 1D FDTD is showed in Fig 2.3, which is redrawn by PowerPoint[17].
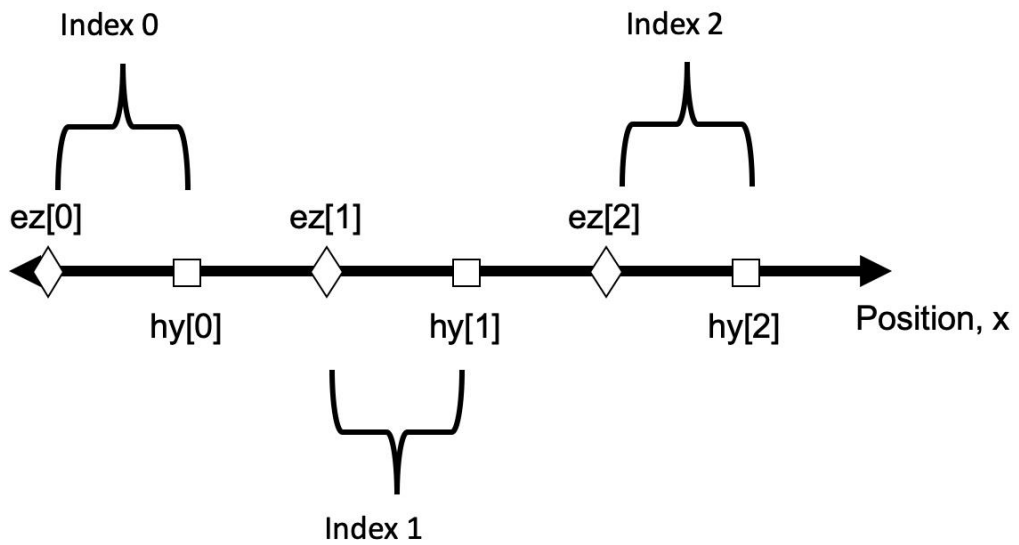

Figure 2.3. The 1D FDTD for Computational Analysis [17]

As in the approximated Equations 2.31 and 2.34, the programmable versions of the FDTD becomes,

hy[mm] = hy[mm] + (ez[mm + 1] - ez[mm]) / imp0;
ez[mm] = ez[mm] + (hy[mm] - hy[mm - 1]) * imp0;

A wave source provides a propagation of light into the structure while the iteration of the EM waves with the FDTD method . Regarding Maxwell's Equation 2.4, the displacement vector is the outer current flow inside the loop. Therefore, it can be adapted for the source propagation for the FDTD method. Equation can be manipulated as follows [18, 19, 29],

$$\frac{\partial \vec{E}}{\partial t} = \frac{1}{\epsilon} \nabla \times \vec{H} - \frac{1}{\epsilon} \vec{J} \tag{2.39}$$

For the computational world, Equation 2.39 can be interpreted as follows,

$$E_z^{q+1}[m] = E_z^q[m] + \frac{\Delta_t}{\epsilon \Delta_x} \left(H_y^{q+\frac{1}{2}}\left[m+\frac{1}{2}\right] - H_y^{q+\frac{1}{2}}\left[m-\frac{1}{2}\right] \right) - \frac{\Delta_t}{\epsilon} J_z^{q+\frac{1}{2}}[m] \tag{2.40}$$

for the conservation of the field update, the discrete form can be rearranged as follows,

$$E_z^{q+1}[m] = E_z^q[m] + \frac{\Delta_t}{\epsilon \Delta_x} \left(H_y^{q+\frac{1}{2}}\left[m+\frac{1}{2}\right] - H_y^{q+\frac{1}{2}}\left[m-\frac{1}{2}\right] \right) \tag{2.41}$$

$$E_z^{q+1}[m] = E_z^{q+1}[m] - \frac{\Delta_t}{\epsilon} J_z^{q+\frac{1}{2}}[m] \tag{2.42}$$

The discrete Equation 2.42 gives a clue for the source implementation of the FDTD method. While running the discrete equations, it is observed that the source is moving which is not fit for experimental study. Therefore, the absorbing boundary condition (ABC) is used to limit the spatial grid [18, 29, 37]. In 1D FDTD, the ABC is implemented by equality of first two grids of electric field (ez [0] = ez [1]) and last two girds of magnetic field (hy[mm] = hy[mm-1]). Then the fields are no longer reflected in the structure. The fields reaching the ends of the grid is disappearing after the ABC.

There is still a problem with the FDTD method. After running the simulation. The wave is propagating in both the left and right direction. Only the right one should limit this propagation. Therefore, the total field/scattered field boundary is used [18, 29, 37]. This boundary divides the point at which source is added, into two as total field

and scattered field [17-19,29]. If Equation 2.34 is taken, the additional magnetic term is called a total field source and the minus one is called a scattered field source.

$$E_z^{q+1}[m] = E_z^q[m] + \frac{\Delta_t}{\epsilon \, \Delta_x} \left(H_y^{q+\frac{1}{2}}\left[m + \frac{1}{2}\right] - H_y^{q+\frac{1}{2}}\left[m - \frac{1}{2}\right] \right) \qquad (2.34)$$

For the 1D FDTD method, the scattered field can be prevented by adding an electric field of source into a discrete form of an equation. Then Equation 2.34 becomes,

$$E_z^{q+1}[m] = E_z^q[m] + \frac{\Delta_t}{\epsilon \, \Delta_x} \left(H_y^{q+\frac{1}{2}}\left[m + \frac{1}{2}\right] \right)$$

$$- \frac{\Delta_t}{\epsilon \, \Delta_x} (H_y^{q+\frac{1}{2}}\left[m - \frac{1}{2}\right] - \frac{1}{\eta} E_z^{src}[m - \frac{1}{2}, q + \frac{1}{2}] \qquad (2.43)$$

As a result, with the help of the TFSF boundary, the wave propagates in the only right direction. By eliminating the scattered field with interference of the source field, the undesired scattered field is eliminated [18, 29, 37].

The nonlinear conditions determine the experimental circumstances. Since the FDTD method provides free space propagation so far, it must be available for different mediums and conditions. Regarding Equations 2.31 and 2.34, the coefficients relate to the properties of mediums. Therefore, by arranging Equations by adding the terms of μ_r and ϵ_r, the medium conditions can be met. Also, it is known that experimental conditions result in loss [17, 18, 37]. Therefore, for the reality, the loss factors should be implemented to the FDTD method. Equations 2.4 has conductivity with current density. If equation is manipulated concerning conductivity, Equation becomes

$$\nabla \times \vec{H} = \frac{\partial \vec{D}}{\partial t} + \sigma \vec{E} \qquad (2.44)$$

23

Then if the approximation is held, the loss factor becomes in discrete form as,

$$E_z^{q+1}[m] = \frac{E_z^{q+1}[m] + E_z^q[m]}{2} \tag{2.45}$$

By manipulating Equation 2.34 by adding loss factor, Equation is,

$$E_z^{q+1}[m] = \left(\frac{1 - \frac{\sigma\Delta_t}{2\epsilon}}{1 + \frac{\sigma\Delta_t}{2\epsilon}}\right) E_z^q[m]$$

$$+ \frac{\frac{\Delta_t}{\epsilon \Delta_x}}{1 + \frac{\sigma\Delta_t}{2\epsilon}} \left(H_y^{q+\frac{1}{2}}\left[m + \frac{1}{2}\right] - H_y^{q+\frac{1}{2}}\left[m - \frac{1}{2}\right]\right) \tag{2.46}$$

For the magnetic field, the same operations are held. Regarding Equation 2.3, for adding loss factors, it becomes,

$$\nabla \times \vec{E} = -\mu\frac{\partial\vec{H}}{\partial t} - \sigma_m\vec{H} \tag{2.47}$$

After manipulations as in an electric field, the loss magnetic field equation is as follows [17, 18, 37].

$$H_y^{q+1}\left[m + \frac{1}{2}\right] = \left(\frac{1 - \frac{\sigma_m\Delta_t}{2\mu}}{1 + \frac{\sigma_m\Delta_t}{2\mu}}\right) H_y^{q-\frac{1}{2}}\left[m + \frac{1}{2}\right]$$

$$+ \frac{\frac{\Delta_t}{\mu \Delta_x}}{1 + \frac{\sigma_m\Delta_t}{2\mu}} \left(E_z^q[m + 1] - E_z^q[m]\right) \tag{2.48}$$

The FDTD method is a flexible method to analyze EM waves. The closed discrete forms of Maxwell's equations are the basis of the method. However, for compromising the experimental conditions, some of the improvements should be made. The method has no restrictions for sources. Any source can be implemented. So, after update for loss mediums, the method can be applied for any material. Although the discrete forms are taken as linear medium, in discrete time and space, the method can be adapted for any medium at that time the medium changes.

In this chapter 1D, the FDTD method is interpreted from Maxwell's equations regarding Yee Cell [17, 18, 26, 37]. As discussed in the introduction part, the FDTD method itself does not respond to non-stationary objects. Therefore, as in the literature survey part, Q. Jiang proposed a dynamical form of the FDTD method in which the position of PhC varied by manipulating the dielectric constant and magnetic permeability at each temporal step. The C++ coded dynamic FDTD method is also based on the idea of the manipulation of the material specifications. Since the proposed method is a kind of the FDTD method, it is composed of Yee Cells.

Moreover, the proposed method can simulate the dynamical change of the refractive index of the structure. It is discussed at the beginning of Chapter 2 that the iteration of the EM fields is following each other values. At each time slots, the EM fields are re-calculated with their previous values.

The interpretation of the dynamic method can be manipulated by using the coefficients as in Equations 2.31 and 2.34. Therefore, the change in the refractive index results in a manipulation of these coefficients. At each time slot, these coefficients are measured concerning the dynamical tunings. However, these coefficients depend on the courant number and grid size. Therefore, regarding the stability issues, the change should be limited. Since the grid size is 25 nm, the corresponding refractive index change for the silicon is limited between the values 2.4103 and 4.3396. The following structures, double microring resonator, and L3 coupled cavity PhC are simulated inside this range. However, regarding the EIT case, as discussed at the beginning of the

introduction, the tune is limited as less than this range. Therefore, the excess of the limits is not required to deal with it.

The proposed method, as indicated before is based on the Yee cell. Therefore, it can simulate the structures, double microring resonator and L3 coupled cavity PhC with a conventional method as well. Also, the method is used to simulate the dynamic tuning cases for the EIT issue. Therefore, the following chapters give the detailed simulations results of the proposed method with comparative results with both experimental and conventional FDTD methods.

CHAPTER 3

THE INTEGRATED COUPLING OF DOUBLE MICRORING RESONATOR AND THE VERIFICATION OF THE PROPOSED FDTD METHOD

3.1. The Structure of Ring Resonator

The simple ring resonator is an optical device that consists of a waveguide and ring waveguide as in Fig. 3.1. The resonator works as coupling with the outer of the ring waveguide. The structure in the Fig 3.1 which is redrawn by the proposed FDTD method based simulation code, has the mechanism of coupling of the incident field, propagating along the waveguide, with ring waveguide.
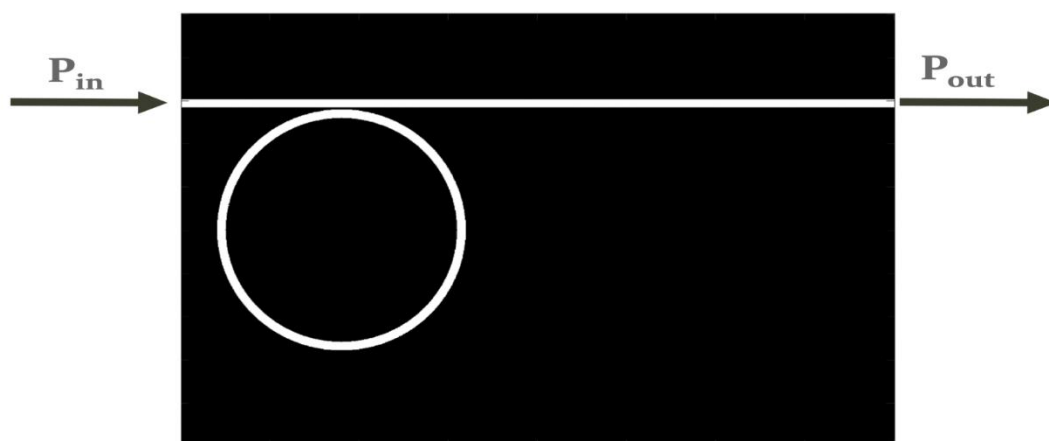
Figure 3.1. Single Ring Resonator [11,13]

This mechanism works as a spectral filter which can be used as wavelength division multiplexing (WDM) in optical communication [11,13]. Also, for the optical sensing, the transmission spectrum of the ring resonator gives a dip around the desired wavelength. This spectral filter structure can be used as an add-drop filter and an all-

pass filter, which are shown in the Fig 3.1 and 3.2 respectively, redrawn by the proposed FDTD method based simulation code. Once the light is passing through the resonator, it will be added or dropped depending on its wavelength [13].

To obtain the transmission from the resonator, the ratio of input and output electric field is calculated. The ratio is [38],

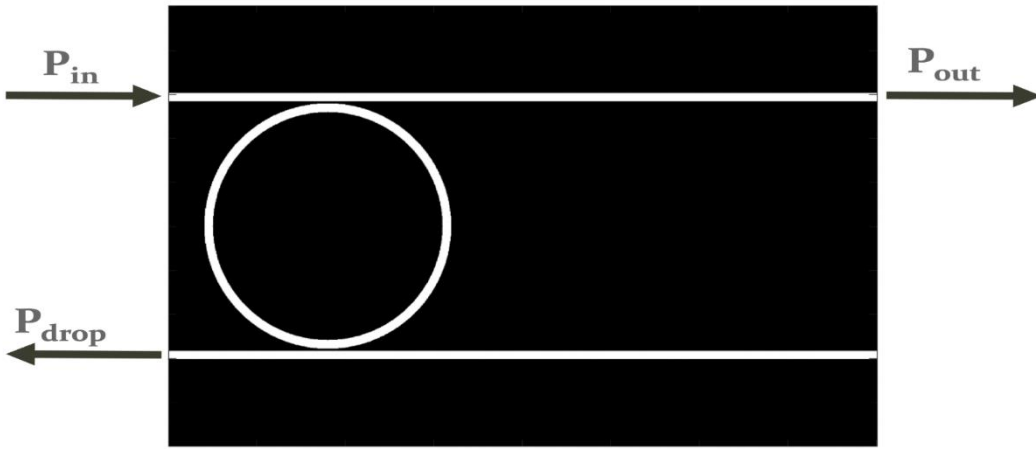$$\frac{\vec{E}_{pass}}{\vec{E}_{in}} = e^{i(\pi+\phi)} \frac{a - re^{-i\phi}}{1 - rae^{-i\phi}} \tag{3.1}$$

Figure 3.2. The Add-Drop Filter [11,13]

The transmission which is equal to square of Equation 3.1 is obtained as [38],

$$T = \left(\frac{\vec{E}_{pass}}{\vec{E}_{in}}\right)^2 = \frac{a^2 - 2racos\phi + r^2}{1 - 2racos\phi + (ra)^2} \tag{3.2}$$

It is defined as r is the self-coupling coefficient, and k is the cross-coupling coefficient. Then, assuming no loss observed during the coupling, the conservation is as follows,

$$r^2 + k^2 = 1 \tag{3.3}$$

28

Resonator is the device to resonate with the wavelength of the light in a round trip, $m2\pi$ around the loop of the resonator. Therefore, the transmission of the resonator is repeated in each round of 2π, which is shown in the Fig 3.3.
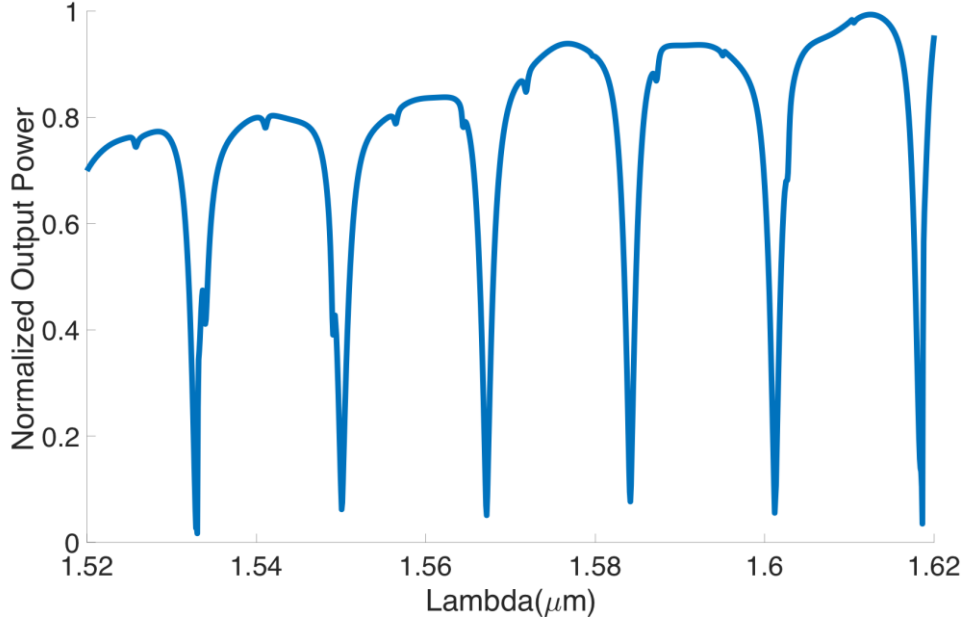

Figure 3.3. Transmission of Add-Drop Filter

There are two transmissions from the add-drop filter. One is for pass transmission, which is in Fig 3.3, and the other is drop transmission. The derived form of the transmission spectrums are [39],

$$T_p = \left(\frac{\vec{E}_{pass}}{\vec{E}_{in}}\right)^2 = \frac{r_2^2 a^2 - 2r_1 r_2 a cos\phi + r_1{}^2}{1 - 2r_1 r_2 a cos\phi + (r_1 r_2 a)^2} \tag{3.4}$$

$$T_d = \left(\frac{\vec{E}_{drop}}{\vec{E}_{in}}\right)^2 = \frac{(1 - r_1{}^2)(1 - r_2{}^2)a}{1 - 2r_1 r_2 a cos\phi + (r_1 r_2 a)^2} \tag{3.5}$$

Here, r_1 is f pass coefficient and r_2 is the drop coefficient.

3.2. The Coupling of Double Microring Resonator

It is showed that a single ring resonator could be used for an add-drop filter. If the ring resonator is doubled, the structure becomes two microring resonator. The Fig 3.4, which is redrawn by the proposed FDTD method based simulation code, shows the structure of two rings resonator.
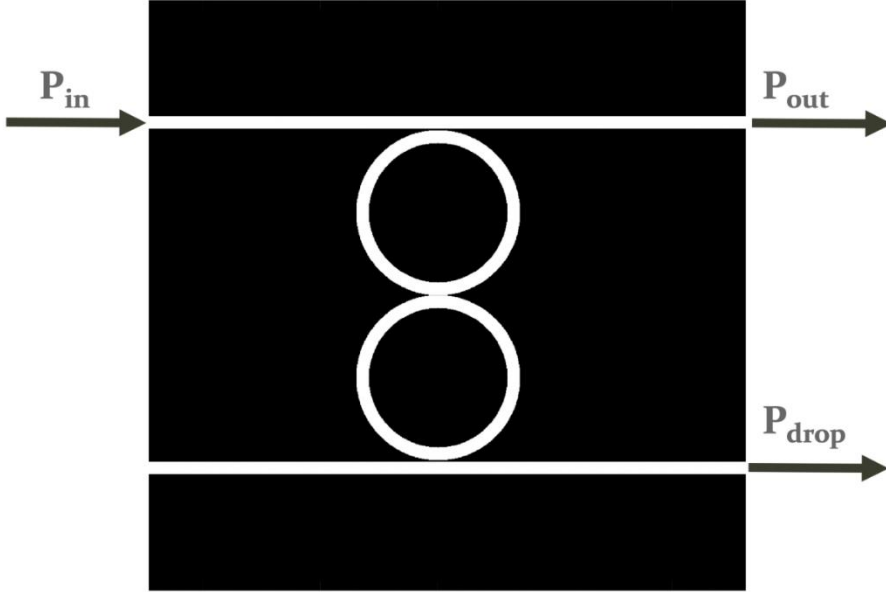

Figure 3.4. Two Ring Resonators [40]

The structure, two rings resonator, is used as a wavelength-selective filter switch. These two rings can be arranged as tune-detune operations. It has the advantage of being able to have extra tuneability. When the rings are detuned, the structure becomes an all-pass filter. So, when the two rings are tuned, the selective wavelength is filtered. Its function is switching depending on the wavelength. It can give a more consistent wavelength-selective result than the single ring resonator. Coupling matrix elements of the structure are [40],

$$H_{21} = \frac{C_1 - C_2 xz^{-1} - C_1 C_2 C_3 xz^{-1} + C_3 (xz^{-1})^2}{1 - C_1 C_2 xz^{-1} - C_2 C_3 xz^{-1} + C_1 C_3 (xz^{-1})^2} \tag{3.6}$$

$$H_{31} = \frac{jS_1 S_2 S_3 xz^{-1}}{1 - C_1 C_2 xz^{-1} - C_2 C_3 xz^{-1} + C_1 C_3 (xz^{-1})^2} \tag{3.7}$$

$$C_i = \frac{[(1-\gamma)(1-\kappa_i)]}{2}, S_i = -j\frac{[(1-\gamma)(\kappa_i)]}{2}, x = e^{-\frac{\alpha L}{2}}, z^{-1} = e^{-j\beta L}, k = 2\pi L, L = 2\pi R$$

This structure is composed of two series connections of the rings. Here, the parallel-connected ring resonator is mainly studied. The parallel-connected double ring resonator is in Fig 3.5, which is redrawn by the proposed FDTD method based simulation code.
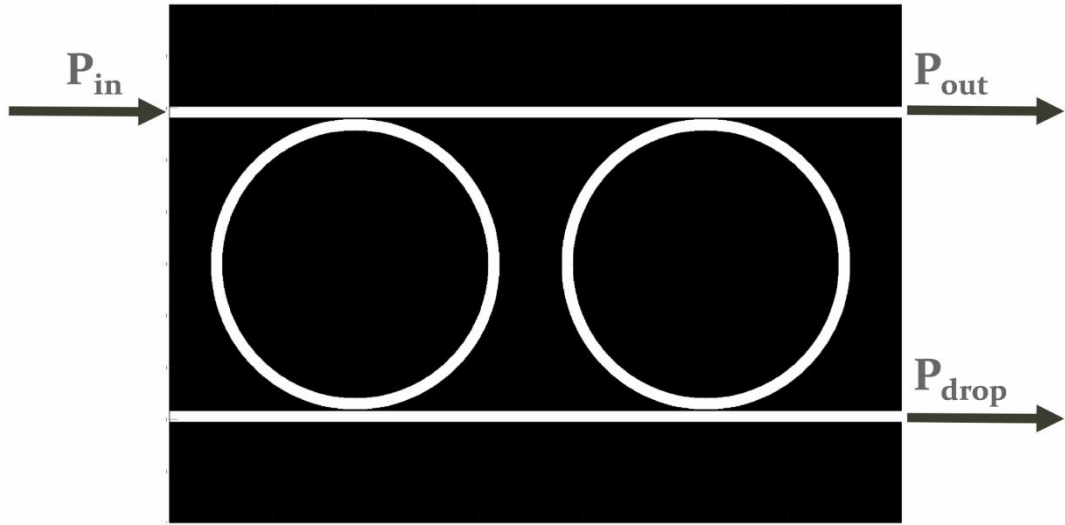

Figure 3.5. The Parallel Connected Double Microring Resonator [6,7,40]

The structure is again working with a tune-detune of rings. Here, the difference of this structure from the parallel one, [40] is the coupling between rings and waveguides. The serial connection of rings rather than parallel represents the continuous add-drop filtering of incident fields from both two ring-waveguide structure is observed. At the on-state which identifies the identical refractive index of rings, light is passing through. In addition, at the off-state which identifies the difference at a refractive index of rings to obtain EIT case, explained in the Introduction chapter, light is stored inside the structure or cavity.

The coupling matrix elements of the ring 1 are [40],

$$H_{11}^1 = \frac{r_1 - r_2^* \left(e^{-\frac{\alpha L}{2}} e^{\frac{j\phi}{2}} \right)^2}{1 - r_1^* r_2^* \left(e^{-\frac{\alpha L}{2}} e^{\frac{j\phi}{2}} \right)^2} \tag{3.8}$$

$$H_{22}^1 = \frac{r_2 - r_1^* \left(e^{-\frac{\alpha L}{2}} e^{\frac{j\phi}{2}} \right)^2}{1 - r_1^* r_2^* \left(e^{-\frac{\alpha L}{2}} e^{\frac{j\phi}{2}} \right)^2} \tag{3.9}$$

$$H_{12}^1 = H_{21}^1 = \frac{-k_1^* k_2 e^{-\frac{\alpha L}{2}} e^{\frac{j\phi}{2}}}{1 - r_1^* r_2^* \left(e^{-\frac{\alpha L}{2}} e^{\frac{j\phi}{2}} \right)^2} \tag{3.10}$$

The coupling matrix elements of the ring 2 are,

$$H_{11}^2 = \frac{r_3 - r_4^* \left(e^{-\frac{\alpha L}{2}} e^{\frac{j\phi}{2}} \right)^2}{1 - r_3^* r_4^* \left(e^{-\frac{\alpha L}{2}} e^{\frac{j\phi}{2}} \right)^2} \tag{3.11}$$

$$H_{22}^2 = \frac{r_4 - r_3^* \left(e^{-\frac{\alpha L}{2}} e^{\frac{j\phi}{2}} \right)^2}{1 - r_3^* r_4^* \left(e^{-\frac{\alpha L}{2}} e^{\frac{j\phi}{2}} \right)^2} \tag{3.12}$$

$$H_{12}^2 = H_{21}^2 = \frac{-k_3^* k_4 e^{-\frac{\alpha L}{2}} e^{\frac{j\phi}{2}}}{1 - r_3^* r_4^* \left(e^{-\frac{\alpha L}{2}} e^{\frac{j\phi}{2}} \right)^2} \tag{3.13}$$

The coupling matrix elements of the waveguide length L_w are,

$$G_{11} = e^{j\theta} \tag{3.14}$$

$$G_{22} = e^{-j\theta} \tag{3.15}$$

$$G_{12} = G_{21} = 0 \tag{3.16}$$

3.3. The Experimental Model of Double Ring Resonator

The Double Ring Resonator is the focus of the proposed dynamic FDTD method. The structure is simulated with both the conventional and the proposed dynamical FDTD. A double microring resonator is experimentally analyzed with a dynamic tune of the rings. With the help of a dynamic tune, the light is stored inside the resonator. As mentioned in the introduction chapter, M. Lipson, Q. Xu, and their research group achieved a dynamic tune with altering the refractive index [7]. Besides that, they also changed the diameter of the ring to create a dynamic tune [6]. However, these two works did not mention these changes in their FDTD simulation works. Here, the dynamic tune of FDTD simulation is demonstrated by using these experimental studies.
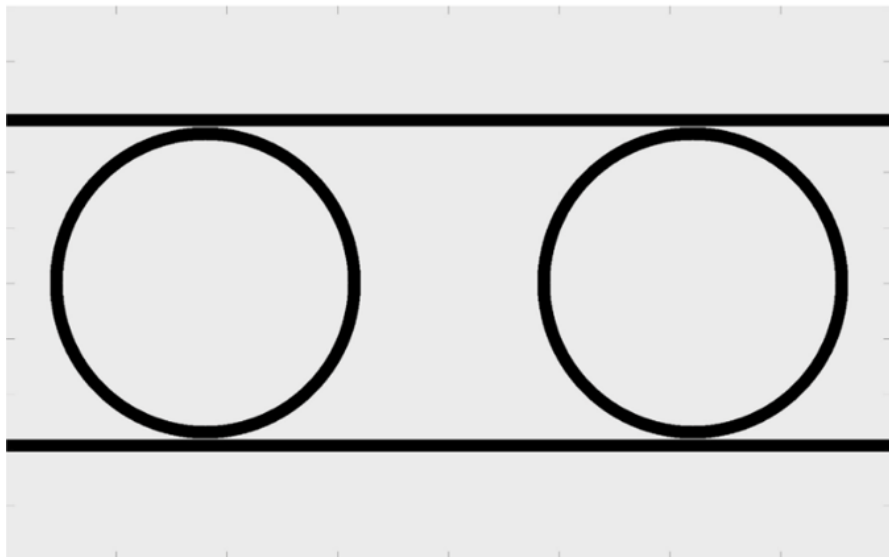

Figure 3.6. The Simulated Double Ring Resonator [6,7]

The FDTD simulation results are compared with an open software MEEP. Therefore, results can be corrected with the conventional method. The proposed dynamic FDTD method is coded with C++ using free XCODE. The plots are obtained with MATLAB R2018a with a license.

The double ring resonator is shown in the Fig 3.6, which is redrawn by the proposed FDTD method based simulation code. The structure has 40 μm length and less than 25 μm width. Each ring waveguides have 7 μm radius, and center to center distance of the rings is 22 μm as in the experimental fabrication [7]. The width of waveguides is 560 nm. The distance between the ring and the waveguide is 65 nm. The structure is composed of silicon with an effective refractive index of 3.3734. The Gaussian pulse is used with a 21 ps length at 1550 nm which is shown in the Fig 3.7.
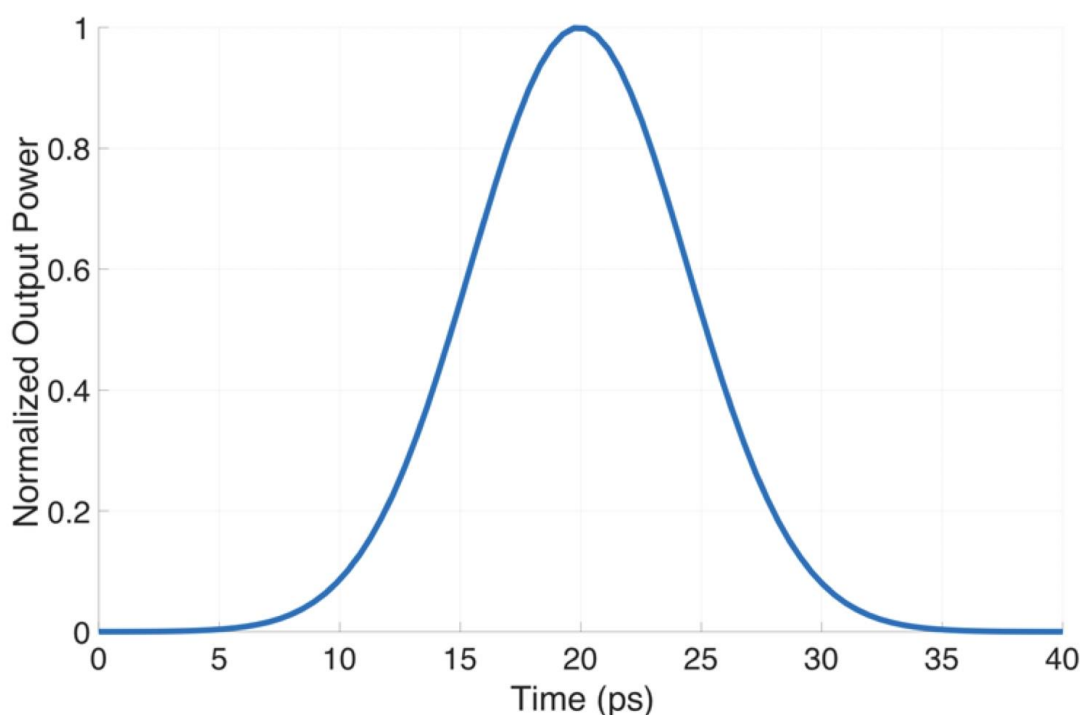
Figure 3.7. The Proposed Gaussian Source

3.4. The Verification of The Proposed Method With Simulation of Double Microring Resonator

The simulation of the double microring resonator is running with using transmission results from MEEP and the C++ coded dynamic FDTD method. The Fig 3.8 shows the MEEP results of the double microring resonator. The simulation results are taken with different versions of the structure. When the double microring resonator is in on

state in which light is released, Fig 3.8-a is obtained. In this case, it can be observed that the transmission of the double microring resonator has a more profound result than the transmission of the single ring resonator. This means that a double microring resonator is filtered more accurate than the single one.
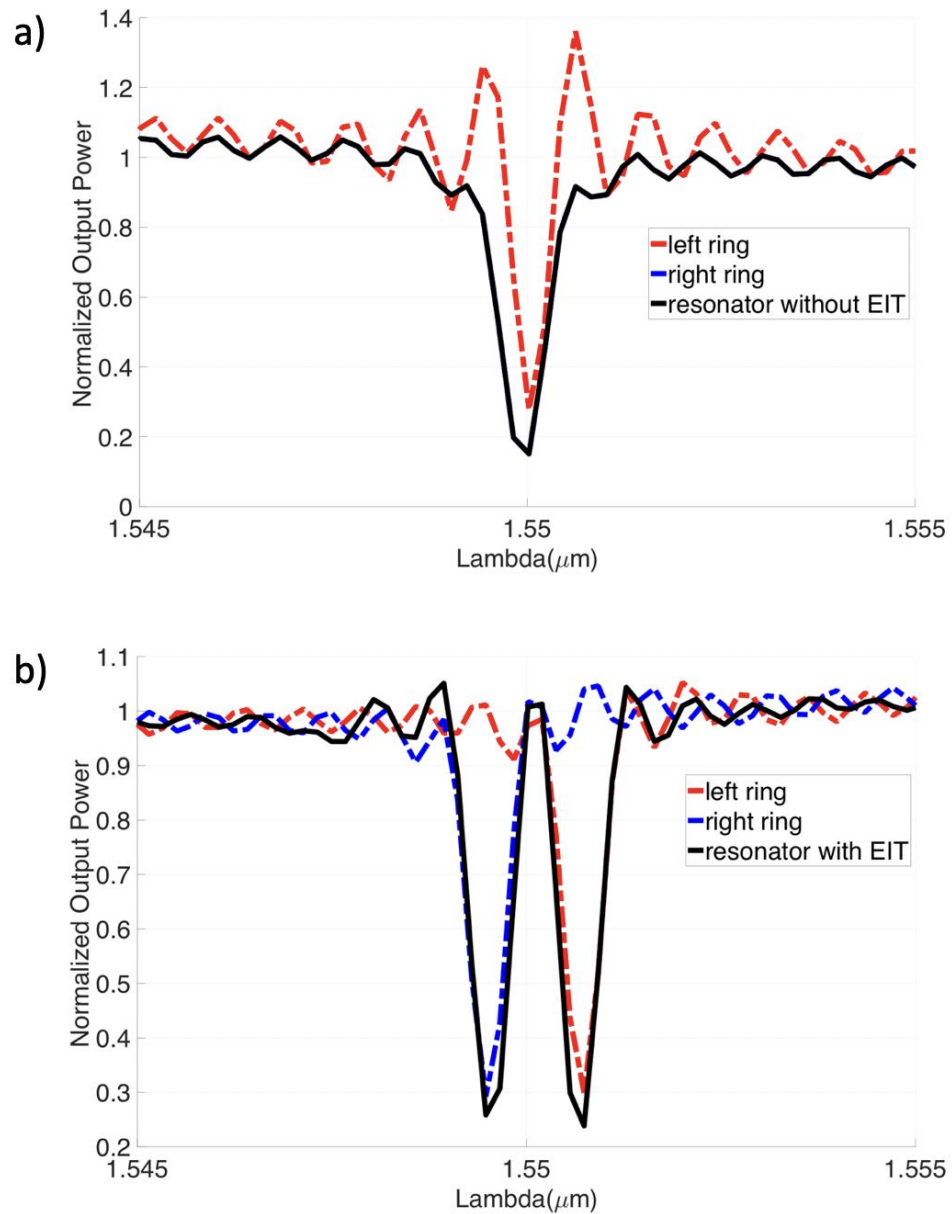

Figure 3.8. The Transmission Results from MEEP. a, The transmission result is taken from the double ring resonator with the identical rings which means the non-EIT case. b, The transmission result is taken from the double ring resonator with the rings, having different effective refractive index, 0.35 nm difference which means EIT case.

In the Fig 3.8-b shows that the off state of the double microring resonator. In this case, light travels around the ring resonator as in the Fig 3.9. There is a difference between the wavelengths as 0.35 nm. The peak at deep transmission occurs in the middle of the transmission of the single ring resonators. In this case, the medium does not affect the light because of the cancellation of electrons inside silicon. The transparency window at this point is called EIT, which is discussed in the Introduction chapter. Experimentally, the EIT case takes 700 ps [7], the lifetime of the light inside the double microring resonator. So, the light is trapped until the tuning maintains. The C++ coded dynamic FDTD method also gives the same results with MEEP. The transmission results of the double microring resonator with the proposed dynamic FDTD are shown in the Fig 3.10.
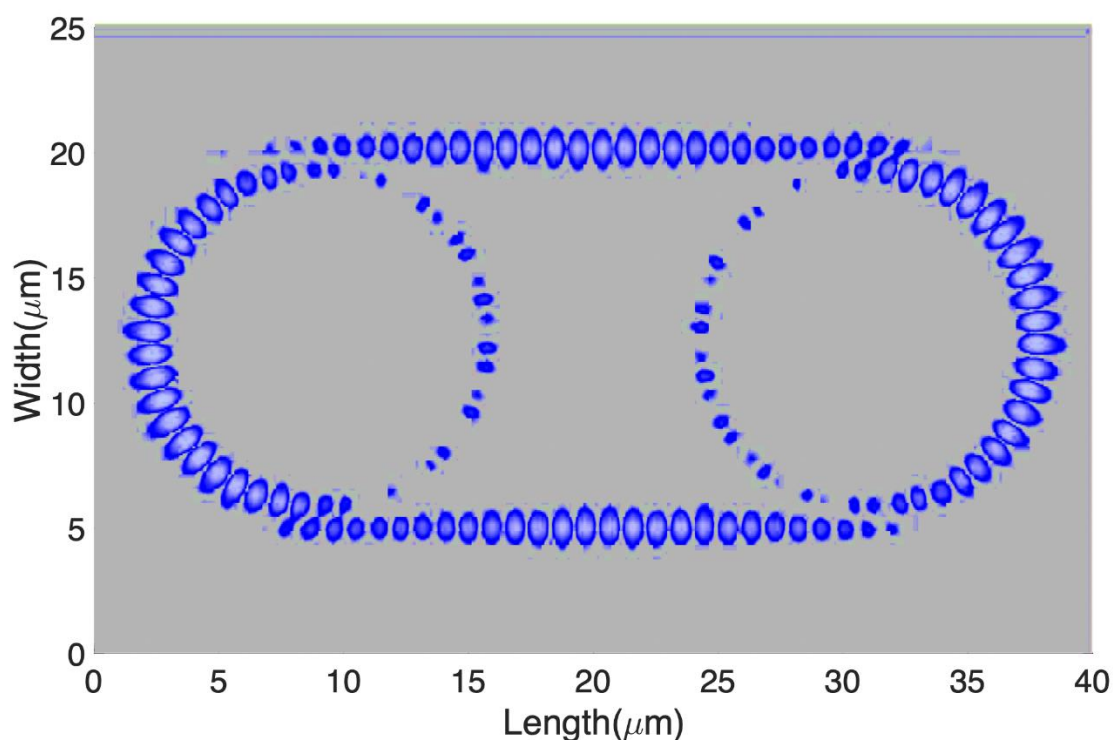

Figure 3.9. Electric Field Distribution of Double Microring Resonator in Off State

The comparison of conventional FDTD, MEEP, and the proposed FDTD results in the similar values of simulation in both non-EIT and EIT cases. This means that MEEP verifies the proposed dynamic FDTD. In Fig 3.10-a, the on-state double microring resonator is shown.
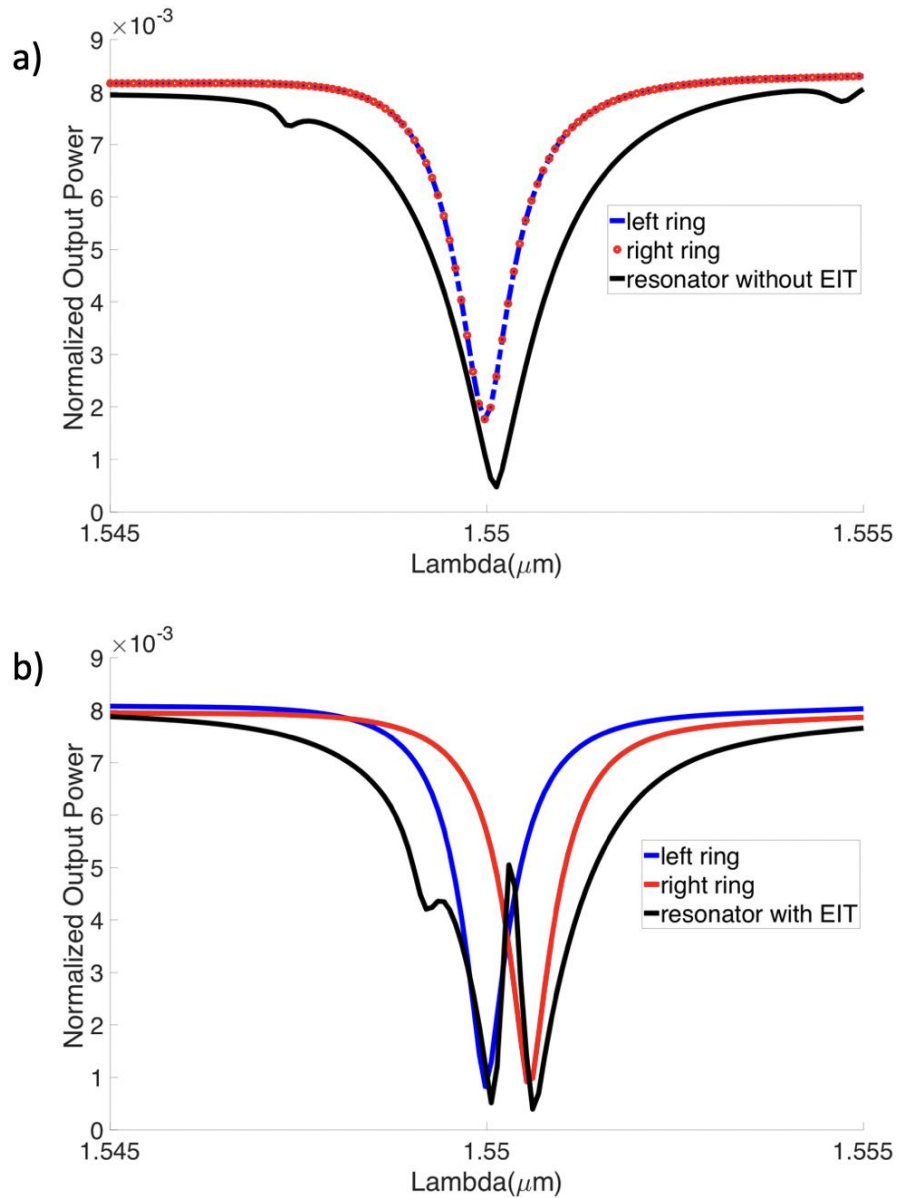

Figure 3.10. The Transmission Results from The Proposed Dynamic FDTD. a, The transmission result is taken from the double ring resonator with the identical rings which means the non-EIT case. b, The transmission result is taken from the double ring resonator with the rings, having different effective refractive index, 0.35 nm difference which means EIT case.

Again, the transmission of the double microring resonator is more profound than the transmission of the single ring resonator. The off-state, when the light traps inside the resonator, gives the result of EIT more accurate. The EIT peak at the transmission deep is observed at $1.55 \ nm$. The wavelength difference is again $0.35 \ nm$, as it equals to variation due to the effective refractive index change which is 3.3708. Xu and his team work also demonstrates the same difference for EIT case. They obtain the EIT case around 1548 nm with a wavelength difference of 0.35nm [6,7]. Comparison of the proposed method can be verified by using the values obtained from MEEP and experimental. So, by comparing the wavelength resonances for the EIT case, the proposed method has similar results with MEEP and experiment [6,7]. To be sure that the obtained results reflect the EIT case, the step by step EIT spectrum is showed in Fig 3.11. There are different cases, depending on the refractive index of the different ring waveguide.
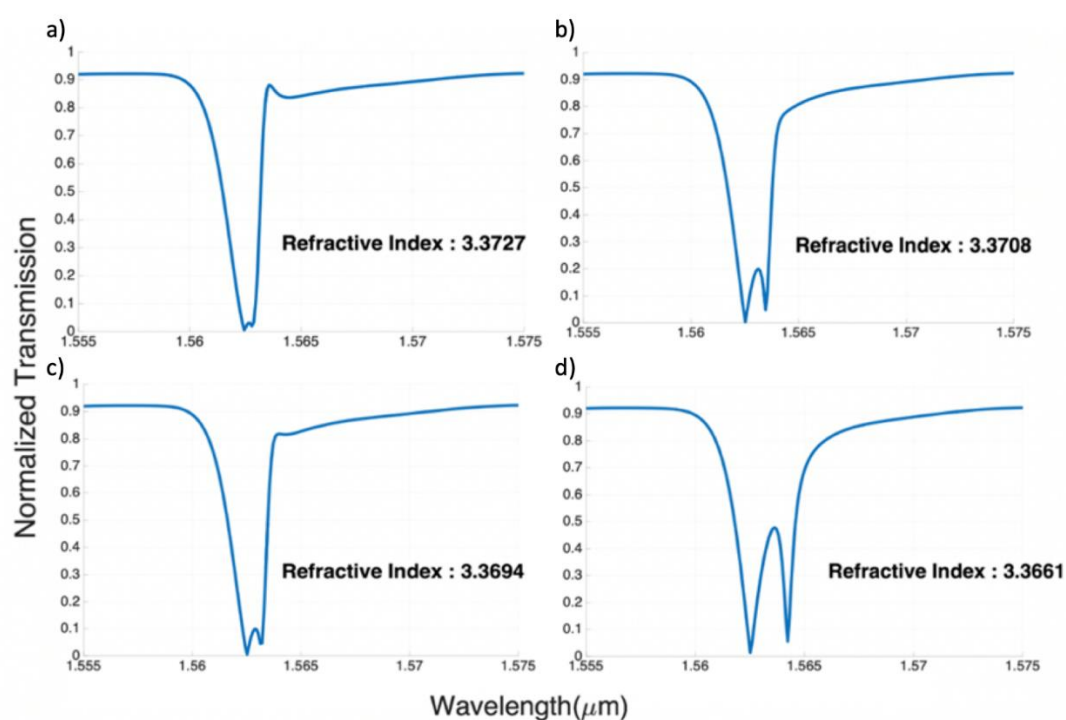

Figure 3.11. EIT Cases Depending on Refractive Index Variations. a, The case represents the non-EIT case with the effective refractive index of one of the rings of 3.3727. b, The case represents the EIT case with the effective refractive index of one of the rings of 3.3708. c, The case represents the non-EIT case with the effective refractive index of one of the rings of 3.3694. d, The case represents the non-EIT case with the effective refractive index of one of the rings of 3.3661.

The Fig 3.11-a shows the case that the effective refractive index is 3.3727. The EIT does not occur. In the Fig 3.11-b, the ring waveguide has a 3.3708 refractive index. In this case, there is an EIT peak. In the Fig 3.11-c, there is a little peak that exists, but it is not enough. The Fig 3.11-d shows the non-EIT case corresponding to the refractive index is 3. 3661. Although there is a peak, in this case, this peak does not infer the EIT case. This peak is caused by interference of the transmission of the resonance of the ring wavelengths. These results are related to the conventional FDTD method. In this method, the structure is illustrated at the beginning of the simulation, and the change does not maintain during the simulation. However, for the simulation of light trapping and releasing, the dynamically tuning is required with the FDTD.
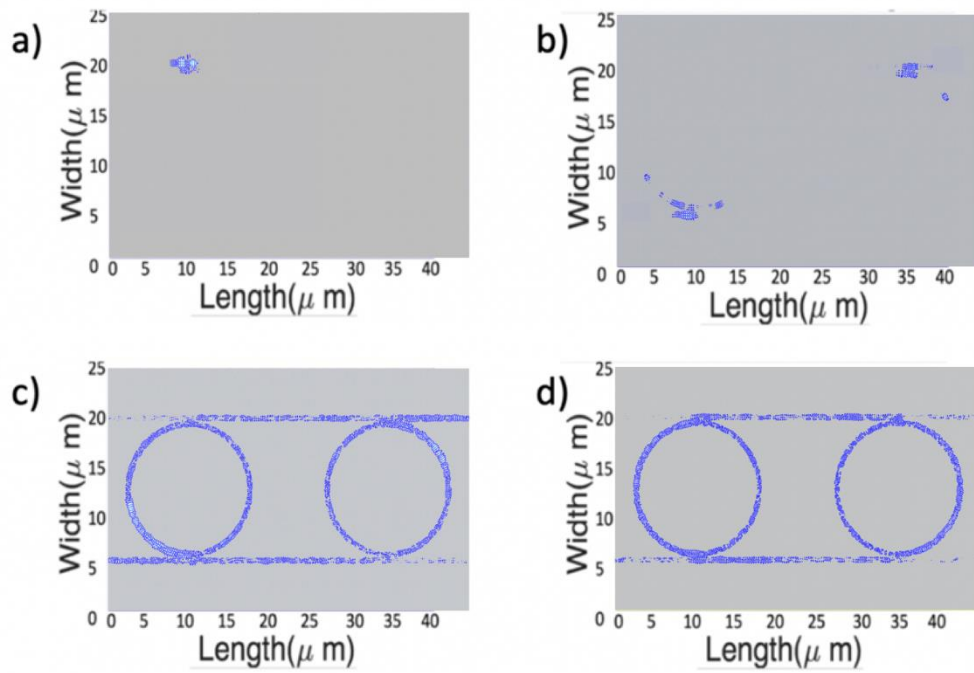

Figure 3.12. Field Distribution of The Dynamical Simulation with The Proposed Method. a, the field distribution at the incident field begins to couple with the resonator. b, The Case for the dynamical tuning occurs which states that the one of the rings has effective refractive index of 3.3708. c, the field distribution for the non-EIT case which has a leakage from the resonator. d, the field distribution for the EIT case which has a continuous travel of the incident light inside the resonator.

39

Since the FDTD method is composed of a set of spatial and temporal grids, between close grids, there can be a function to change the structure. With the help of that idea, the FDTD method is modified as rearranging the structure inside the temporal step. The Fig 3.12 shows that the dynamical FDTD method can change the medium of structure. Each snapshot has illumination parts that state the light passing through the resonator. The light has just arrived in the Fig 3.12-a. After a round trip, it begins to couple with ring waveguides as in the Fig 3.12-b. Just before the dynamic tuning case is shown in the Fig 3.12-c. So, the Fig 3.12-d demonstrates the light trapping case.

To observe the delay of the light, the proposed dynamic FDTD method has time scale results. In the Fig 3.13 – 3.16, different delay times concerning the tuning period are shown. According to these delay times, the light is stored inside the resonator. The Fig 3.13 demonstrates the propagation of light without any delay and dynamic case.
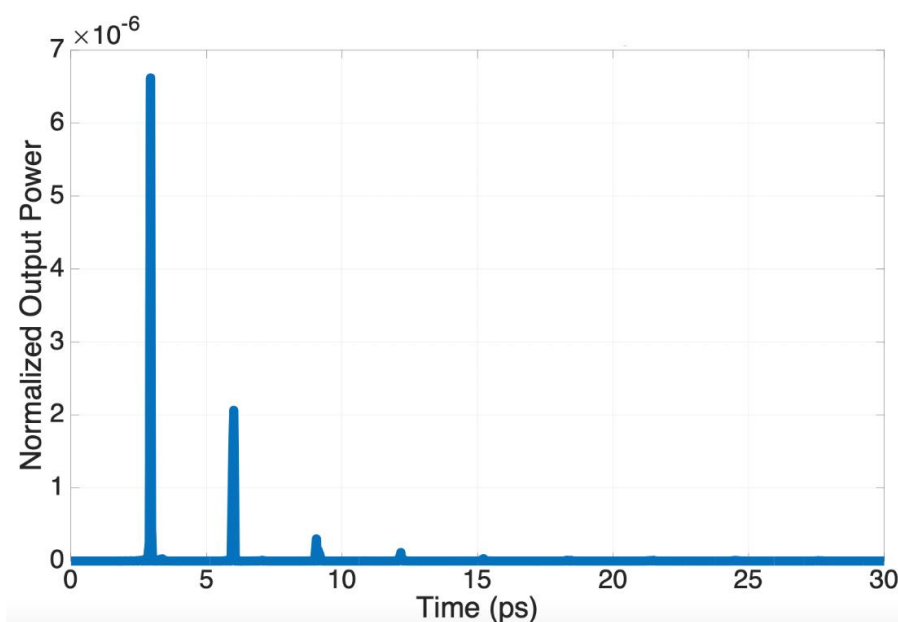

Figure 3.13. Time Scale Pulse Propagation Without Any Delay

In the Fig 3.14, the dynamic period is indicated as an orange line. After the line, the light is releasing, and 15.4 ps delay time is observed. This means that the light travels along the resonator 15.4 ps.
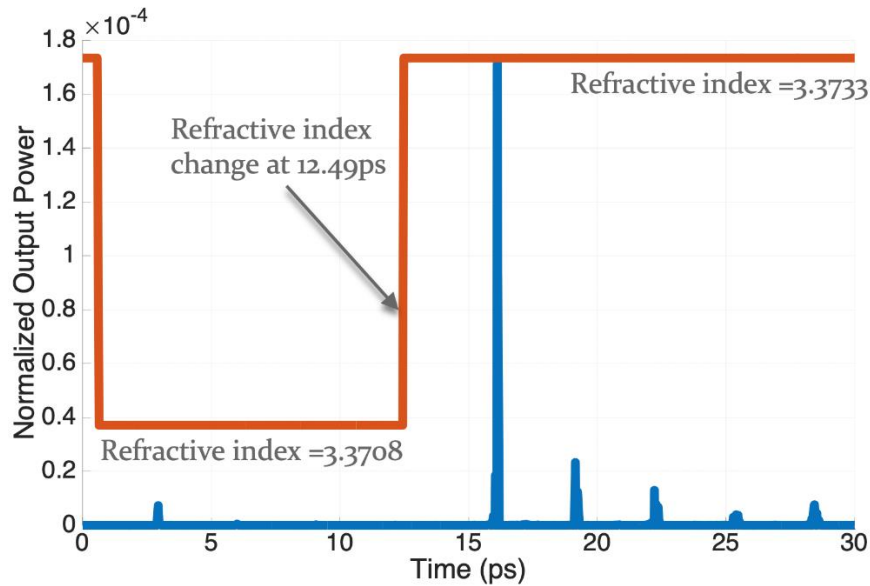

Figure 3.14.Time Scale Pulse Propagation with a Releasing At Time 16.11 ps, Storage Time 15.4 ps

The Fig 3.15 shows a longer storage time. In this case, the light is stored during 20 ps. This means the proposed dynamic FDTD method provides consistent results. In the Fig 3.16, the delayed time is much longer. The light is trapped inside the resonator at the end of 24 ps. The consistent results are corrected with the stable releasing times. The output fields are normalized with the value of the Gaussian source belonging to the Fig 3.7. The waveforms are switched dynamically as the value of the effective refractive index is changed from 3.3733 to 3.3708. These changes are illustrated with the orange line in these figures. It is obtained that these results are consistent with the storage time values. The experimental storage time is obtained as 13 ps in references 6 and 7. Concerning the experimental result, the proposed storage times are applicable for the dynamical FDTD simulation.
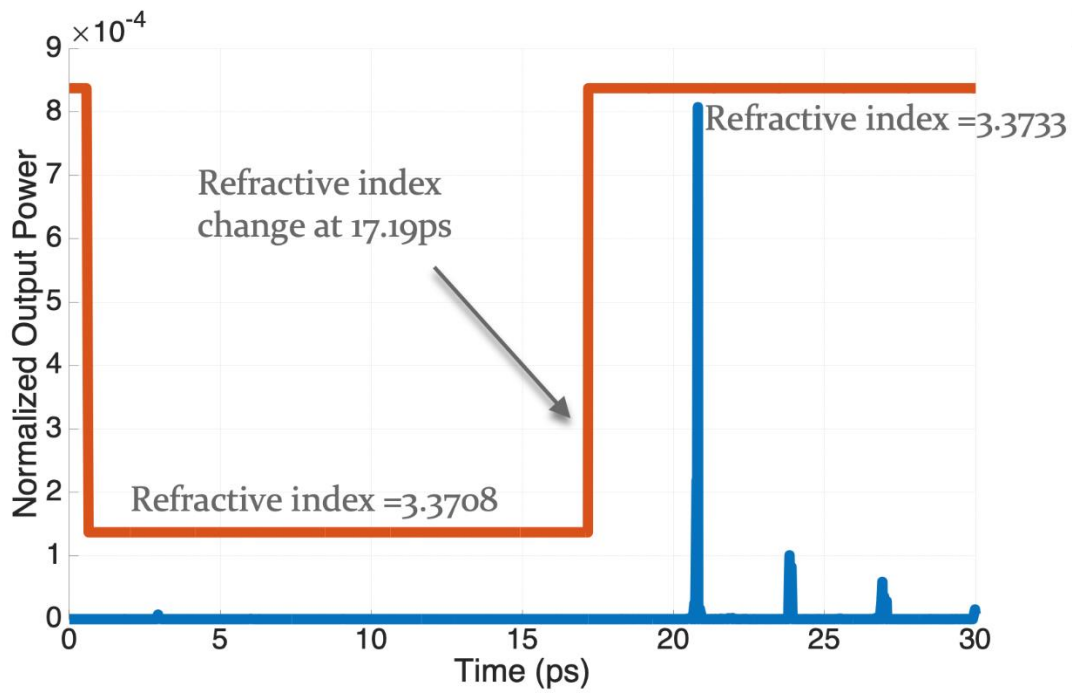
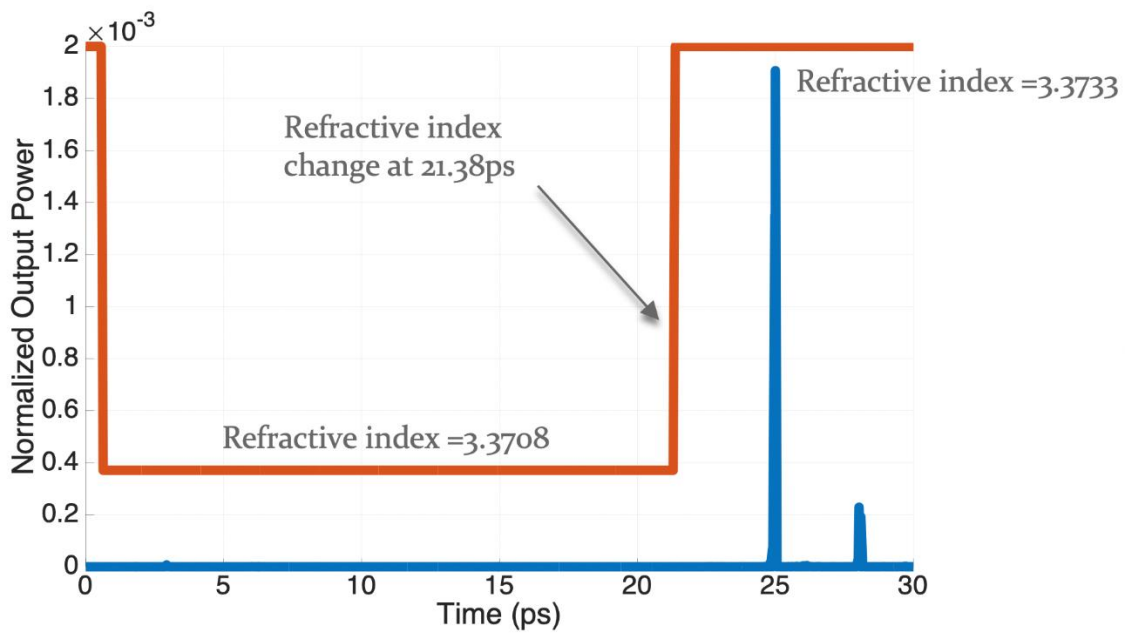*Figure 3.15. Time Scale Pulse Propagation with a Releasing At Time 20.81 ps, Storage Time 20 ps*

Figure 3.16. Time Scale Pulse Propagation with a Releasing At Time 25.0 ps, Storage Time 24.4 ps

42

CHAPTER 4

THE L3 COUPLED CAVITIES PHC AND THE VERIFICATION OF THE PROPOSED FDTD METHOD

4.1. Introduction to Photonic Crystals And Its Properties

Periodicity of molecules and atoms creates a crystal lattice. In a periodic crystal lattice, electrons move through the periodic potential of it. Because of the periodic structure of the lattice, the conductivity of the crystal is limited. This observation means that electrons can have a limited movement and directions inside a crystal lattice. The limitation of the electrons' movement is called the bandgap which is between the energy levels. By following this idea, photonic crystals (PhC) are proposed to control the wave propagation. The bulk PhC structure, in the Fig 4.1, which is redrawn by the proposed FDTD method-based simulation code, provides a propagation of electrons and conduction specification of lattice which means partially forbidden energy levels of electrons [11]. The corresponding band diagram can be seen in the Fig 4.2, which is redrawn by MPB open software. Beyond this idea, photonic crystal (PhC) structures are presented with replacing the electrons with dielectric media. Then, the PhC provides a bandgap for which light is propagating in a certain direction within a specific frequency.
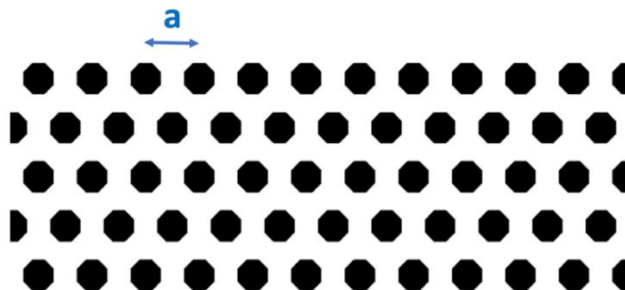

Figure 4.1. A Representative Cartoon of A Bulk PhC [11]

From general aspects of the discrete periodicity of electromagnetic waves, the energy levels in the photonic bandgap can be inferred as Bloch states. If the EM fields are written as dividing from time dependence,

$$\vec{H}(\vec{r}, t) = \vec{H}(\vec{r}).e^{-iwt} \tag{4.1}$$

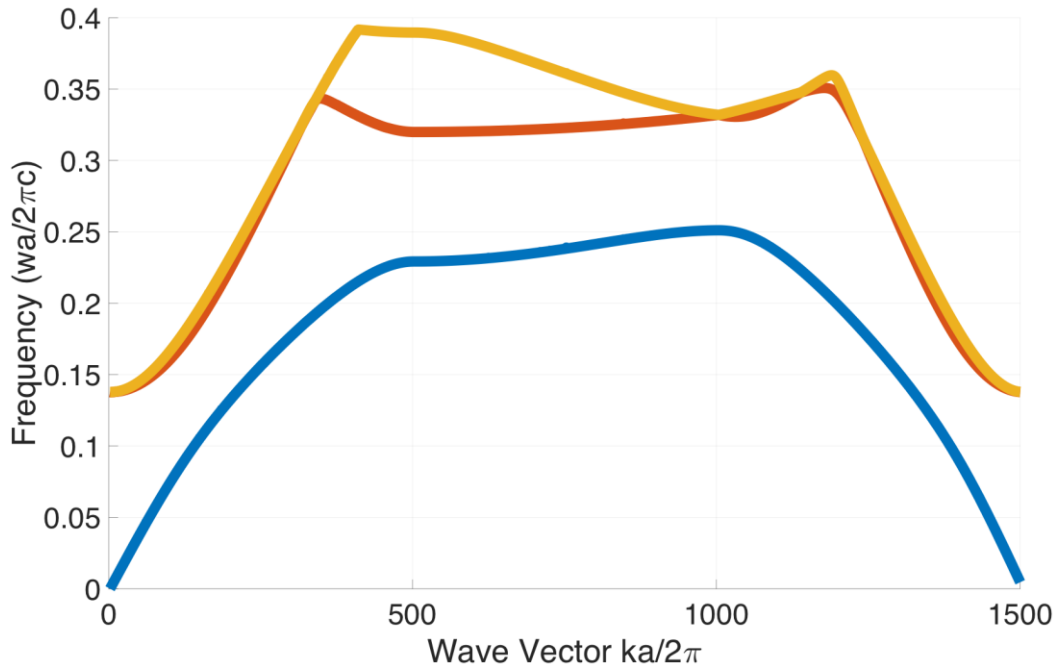$$\vec{E}(\vec{r}, t) = \vec{E}(\vec{r}).e^{-iwt} \tag{4.2}$$

Figure 4.2. Bulk Photonic Crystal Band Diagram [11]

From these fields, rephrased Maxwell's equations become,

$$\nabla \vec{H}(\vec{r}) = 0 \tag{4.3}$$

$$\nabla[\epsilon(\vec{r})\vec{E}(\vec{r})] = 0 \tag{4.4}$$

44

In a simple source-free medium, the EM field equations become transverse. Transverse fields should satisfy the condition of wavefield with also the wave vector. Regarding this condition, the curl equations of Maxwell equations become as,

$$\nabla \times \vec{E}(\vec{r}) - i w \mu_0 \vec{H}(\vec{r}) = 0 \qquad (4.5)$$

$$\nabla \times \vec{H}(\vec{r}) + i w \epsilon_0 \epsilon(\vec{r}) \vec{E}(\vec{r}) = 0 \qquad (4.6)$$

By recovering $H(r)$ from Equations 4.5 and 4.6,

$$\nabla \times \left(\frac{1}{\epsilon(\vec{r})} \nabla \times \vec{H}(\vec{r}) \right) = \left(\frac{w}{c} \right)^2 \vec{H}(\vec{r}) \qquad (4.7)$$

By substituting Equations 4.5 and 4.7,

$$\vec{E}(\vec{r}) = \frac{i}{w \epsilon(\vec{r}) \epsilon_0} \nabla \times \vec{H}(\vec{r}) \qquad (4.8)$$

And,

$$\vec{H}(\vec{r}) = -\frac{i}{w \mu_0} \nabla \times \vec{E}(\vec{r}) \qquad (4.9)$$

Beyond all these continuous translational symmetries is cared regarding modes of operation for analyzing photonic band gaps of PhC [11]. The structure with a translational symmetry does not change its behavior with a shift in position. This property can be defined mathematically as,

$$\vec{T}_{d\hat{z}} e^{ikz} = e^{ik(z-d)} = e^{-ikd} e^{ikz} \qquad (4.10)$$

This is the general form of the eigenvalue. The displacement vector dependence of the eigenvalue can be redefined to obtain the specific wave vector, $\vec{k}$. Then, the magnetic field becomes,

$$\vec{H}_{\vec{k}}(\vec{r}) = \vec{H}_0 e^{i\vec{k}r} \qquad (4.11)$$

This field indicates a set of plane waves. It is indicated that the transverse fields should satisfy the condition of wavefield with also the wave vector. Then, Equation 4.11

should impose $\vec{k} \cdot \vec{H}_0 = 0$. Then, from Equation 4.17, the eigenvalues can be found as,

$$\left(\frac{w}{c}\right)^2 = \frac{|\vec{k}|^2}{\varepsilon} \tag{4.12}$$

and finding the dispersion relation as,

$$w = c\frac{|\vec{k}|}{\varepsilon} \tag{4.13}$$

Considering the infinite plane wave at which the dielectric constant depends on displacement along the z-direction, the wave vector can be written as

$$\vec{k} = k_x \hat{x} + k_y \hat{y} \tag{4.14}$$

In a plane wave, regarding of close points which are at $\vec{r}$, $\vec{r} + d\hat{x}$, $\vec{r} + d\hat{y}$, the symmetry indicates that all points are equal without their phase. Therefore, the wavenumber is an indicated factor. However, with only the value of $\vec{k}$, the plane wave cannot be inferred. As a result, the n is defined to place points at a certain phase, which is a band number. The n, therefore, has a dependence on phase and frequency. So, the n number is proportional to frequency. Then, $(\vec{k}, n)$ is used to call the modes in plane waves.

Photonic crystals are devices such as a discrete form of system because it has a certain permittivity. Therefore, these devices have a discrete form of translational symmetry [11]. In the case of Fig 4.3, which is redrawn by MATLAB, each crystal has a distance a, and thus, the lattice vector becomes $\vec{a} = a\hat{y}$. In the direction of, the structure is infinite. Then, the repetition becomes as $\varepsilon(\vec{r}) = \varepsilon(\vec{r} \pm \vec{a})$. Considering the discrete form, the repetitive distance of lattice is $\vec{R} = l\vec{a}$. Then, the discrete translational symmetry becomes as,

$$\vec{T}_{\vec{R}} e^{ik_y y} = e^{ik_y(y-la)} = e^{-ik_y la} e^{ik_y y} \tag{4.15}$$

The wave vector k_y has a periodicity of $2\pi/a$. Then, the discrete form of magnetic field becomes as,

$$\vec{H}_{k_x,k_y}(\vec{r}) = e^{ik_x x} \sum_m \vec{c}_{k_y,m}(z) \, e^{i(k_y+mb)y} = e^{ik_x x} e^{ik_y y} \sum_m \vec{c}_{k_y,m}(z) \, e^{imby}$$

$$= e^{ik_x x} e^{ik_y y} \, \vec{u}_{k_y,m}(y,z) \tag{4.16}$$

in which $b = 2\pi/a$. It can be inferred that $\vec{u}_{k_y,m}(y,z) = \vec{u}_{k_y,m}(y+la,z)$. This means that the periodicity of the magnetic field in a lattice is Bloch's theorem. In this case, the repetition in k_y value is equal to b. Therefore, the limitation should be arranged as,

$$-\frac{\pi}{a} < k_y \leq \frac{\pi}{a} \tag{4.17}$$

which is called the Brillouin zone. This zone is physically defined as the circle of a lattice point is encountering the space closer to any other one [11].

Bragg-Snell's law is the essential case for the PhC which prevents light, passing through the crystal from destructive interference. Therefore, the light is then diffracted as a result of a reflection at the peak frequency of the photonic bandgap. In the Fig 4.3, the diffraction model in PhC is showed [41]. According to Snell's law,

$$n_1 sin\theta_1 = n_2 sin\theta_2 \tag{4.18}$$

If Equation 4.20 is analyzed as the inequality below,

$$\theta_1 > sin^{-1}(\frac{n_2}{n_1}) \tag{4.19}$$

then, the $sin\theta_2 > 1$ which is impossible. As a result, the critical angle is defined as,

$$\theta_c = sin^{-1}(\frac{n_2}{n_1}) \tag{4.20}$$

while $n_2 > n_1$. The Snell's law implies the conservation of symmetry of w and wave vector $k_{||}$ which is $k_{||} = k sin\theta_1$ and $|\vec{k}| = \frac{nw}{c}$.
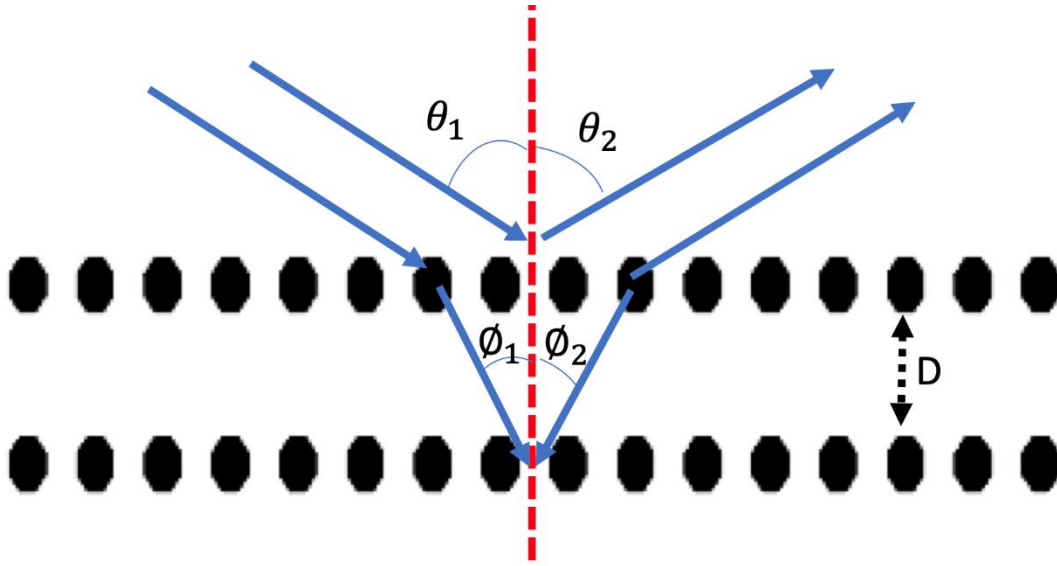
Figure 4.3 Schematics of Snell's Law of Refraction [11,42]

From Snell's law, the diffraction model of the PhC can be modified. Beyond the reflection of light from the surface, the light can also be refracted. In this case, the diffraction photons inside a PhC can be obtained from both Snell's and Bragg's Laws. The Bragg law is

$$m\lambda_m = 2dsin\theta \qquad (4.21)$$

So Snell's Law of refraction is

$$n_1 sin\theta = n_2 sin\varphi \qquad (4.22)$$

combining Equations 4.18 and 4.19,

$$m\lambda_m = 2d\sqrt{n_{eff} - cos^2\emptyset_1} \qquad (4.23)$$

which is the Bragg-Snell Law of refraction [42].

Photonic Crystals are devices that have a photonic bandgap to determine the allowed energy levels. Then, the light is passed through determining its wavelength. The bandgap can be formulated by frequency bands as follows. From Equation 4.16, the eigenvector depending on Brillion zone can be calculated as,

$$\vec{H}_{\vec{k}}(\vec{r}) = e^{i\vec{k}r} \, \vec{u}_{\vec{k}}(\vec{r}) \tag{4.24}$$

at which regarding of rotational symmetry of PhC, $\vec{R} = l\hat{a}_1 + m\hat{a}_2 + n\hat{a}_3$. Substituting Equation 4.24 into Equation 4.7 [42],

$$\nabla \times (\frac{1}{\epsilon(\vec{r})} \nabla \times (e^{i\vec{k}r} \, \vec{u}_{\vec{k}}(\vec{r}))) = \left(\frac{w(\vec{k})}{c}\right)^2 (e^{i\vec{k}r} \, \vec{u}_{\vec{k}}(\vec{r})) \tag{4.25}$$

$$(i\vec{k} + \nabla) \times (\frac{1}{\epsilon(\vec{r})} (i\vec{k} + \nabla) \times \vec{u}_{\vec{k}}(\vec{r})) = \left(\frac{w(\vec{k})}{c}\right)^2 (\vec{u}_{\vec{k}}(\vec{r})) \tag{4.26}$$

Equation 4.26 gives information about the bandgap of PhC. As indicated in the definition of wave vector, n is also determined inside a bandgap. The frequency interval $w(\vec{k})$ has a number as $w_n(\vec{k})$ that indicates the band structure.

4.2. Defect Types on Photonic Crystals And Its Applications

Two-dimensional photonic crystals do not have a gap in the photonic band structure. Therefore, no allowed propagation occurs inside a photonic crystal as in the Fig 4.2. To overcome this issue, defects are created. Defects ruin the symmetry of the PhC [11]. Therefore, the repetition in the periodicity is disturbed.
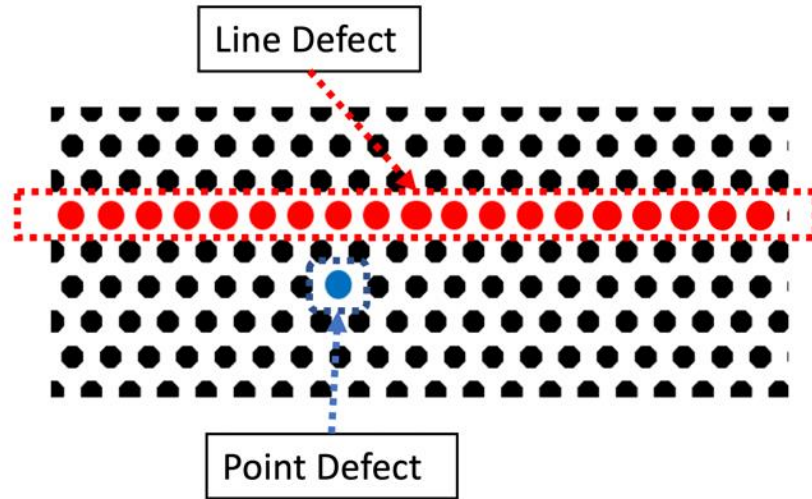

Figure 4.4. Defect Types on 2D Photonic Crystal [11]

49

In 2D, removing a lattice or a row or replacing lattices with dielectric can be used to create defects, as in Fig 4.4, which is redrawn by MATLAB. The defect causes the translational symmetry of the photonic crystal. Therefore, the mode status can be still existing. However, since it is 2D, the symmetry around z-axis is held ($k_z = 0$). So, TE and TM modes can still decouple around the defect [11]. Then, evanescent waves occur inside a defect.

A point defect is a type of defect that causes a single point perturbation. At that point, the light is propagating in-plane of 2D PhC. The structure of the point defect can be seen in the Fig 4.5, which is redrawn by the proposed FDTD method-based simulation code, at which the light is decaying while propagating away from the point defect as concluding in Equation 4.16.
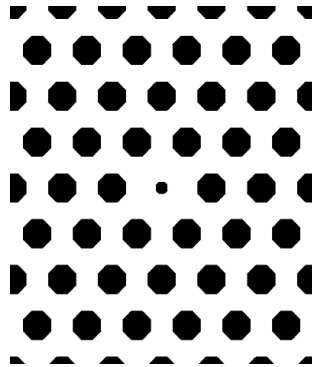
Figure 4.5. Point Defect on PhC [11]

Depending on the defect on that point the band diagram behaves differently. As stated before, the defect can be created as replacing with a different medium. The medium can be high or low compared with the PhC. As given in Equation 4.26, the change in dielectric constant causes of an up/down of the band diagram. The smaller dielectric constant gives a band diagram as in the Fig 4.6 and higher dielectric causes of the band diagram in the Fig 4.7, which are redrawn by MPB. Since band diagrams differ, the spectra are, too. The spectrum related to smaller dielectric point defects has monopole, and the greater one has quadrupole spectrum [11] as seen in the Figs 4.8 and 4.9, which is redrawn by the proposed FDTD method-based simulation code, respectively. These field distributions are normalized with the given Gaussian source.
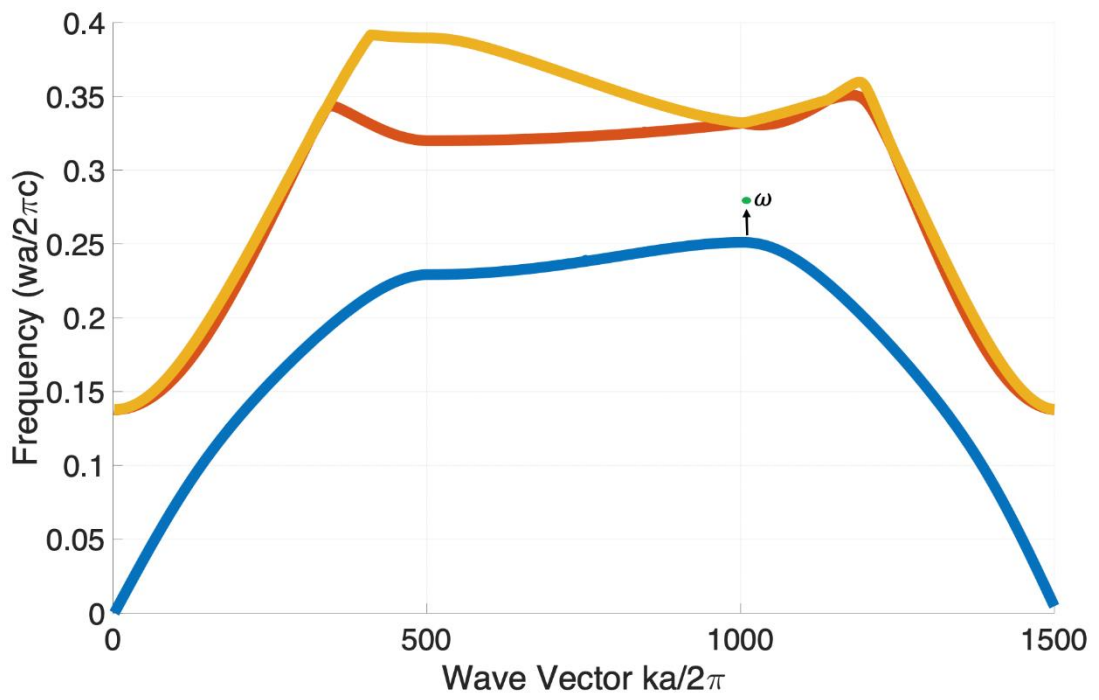
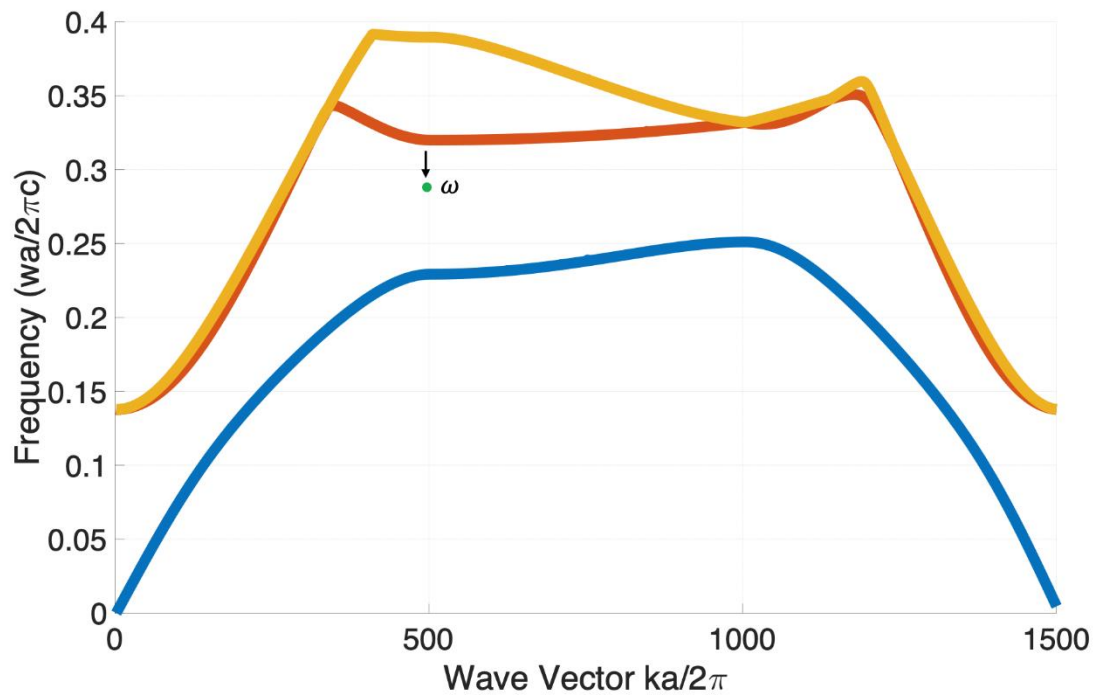*Figure 4.6. Smaller Dielectric Point Band Diagram [11]*

Figure 4.7. Greater Dielectric Point Band Diagram [11]
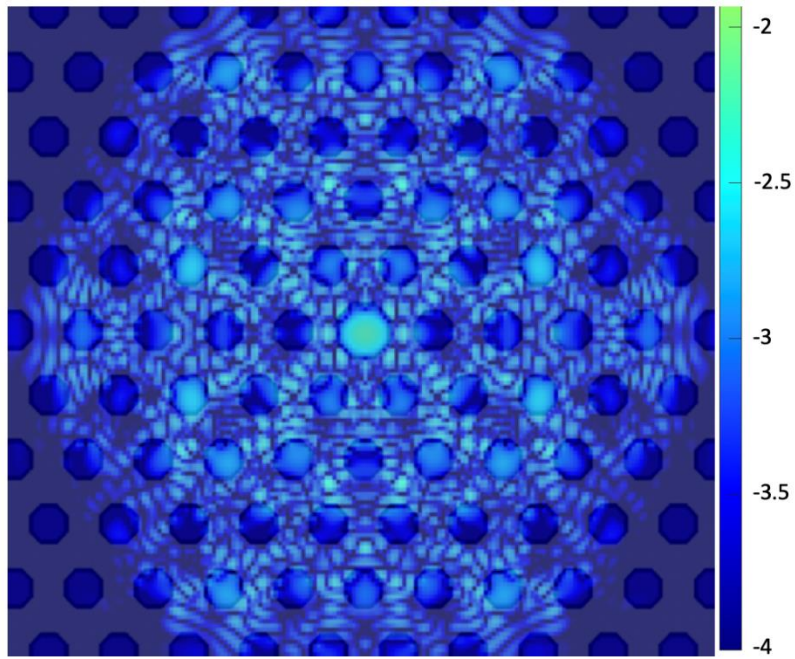
51

Figure 4.8. Electric Field Distribution of Monopole Point Defect PhC [11]
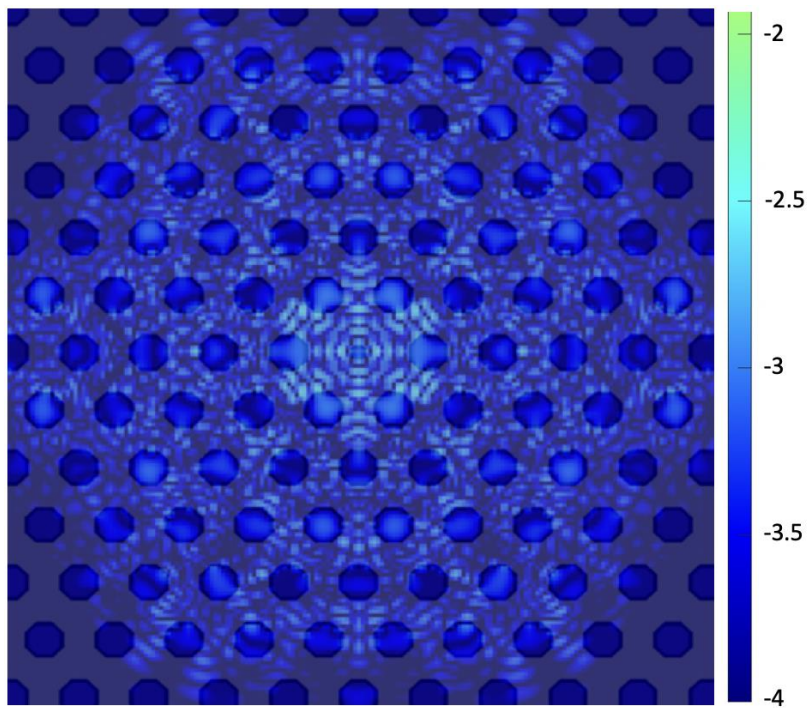

Figure 4.9. Electric Field Distribution of Quadrupole Point Defect [11]

From the view of the point defect PhC, the light propagates inside that point. This means that light is trapped inside the defect until it reaches its lifetime. Besides that, idea, the light can be guided by introducing defects. Such an application is a linear defect type PhC which can be seen from the Fig. 4.10, which is redrawn by the proposed FDTD method-based simulation code.
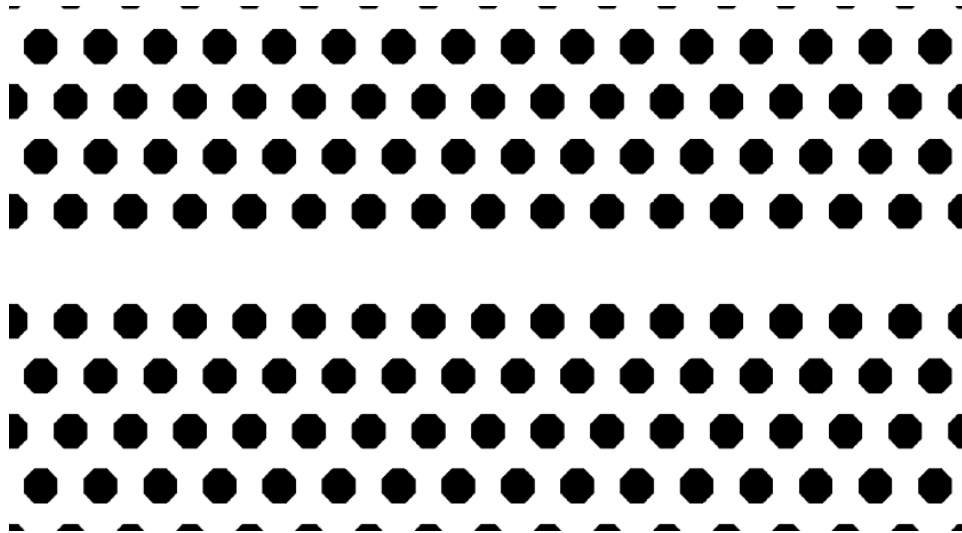

Figure 4.10. Linear Defect on PhC [11]

This type of application is different from the point one with symmetry. Linear defect can preserve the translational symmetry. Inside a point defect, the frequency of mode can be localized regarding inside a photonic bandgap. However, in this case, the wave vector is essential. Not only the frequency of mode determines the light propagation but also the wave vector has an impact. Therefore, this kind of application is called a waveguide. The spectrum analyses of the PhC waveguide is in the Fig 4.11, which is redrawn by the proposed FDTD method-based simulation code. If the PhC is inside a vacuum, there are some advantages, such that regarding Bragg-Snell law as in Equation 4.23, the light passing through the waveguide, interacts with surface layers less than other applications. This means that the losses, causing absorption or nonlinearities are reduced. There are linear defects on PhC, such as removing single or multi rows. Depending on the number of rows removed, the mode of the light

changes [11]. Single-mode waveguides have only one removed row and vice versa. However, multi-mode waveguides have some drawbacks such that multi modes create various group velocity of waves. In this case, the modal dispersion occurs during propagation which is undesirable for transmission applications.
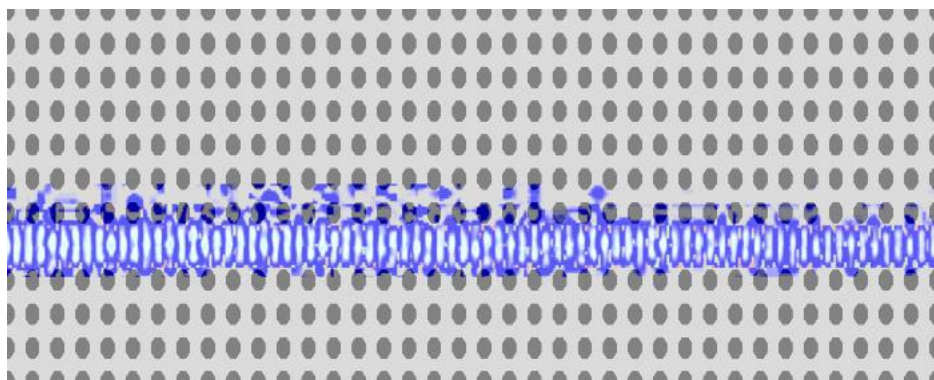

Figure 4.11. Spectrum of The PhC Waveguide [11]

Some applications have both types of defects such that combining both point and linear defects can be used as splitters, crossings or channel drop filters. The waveguide splitter is a device to divide input light other channels [43]. In this case, losses causing absorption are discarded. However, the reflection losses are determined factors. The waveguide splitter is seen in the Fig 4.12 which is redrawn by the proposed FDTD method-based simulation code.
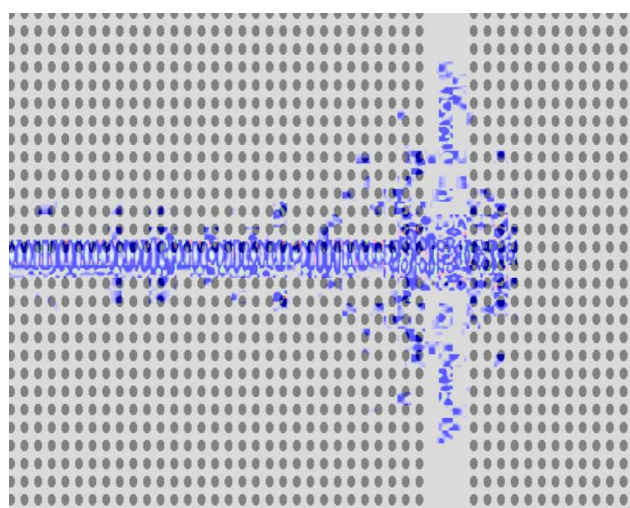

Figure 4.12. Waveguide Splitter [43]

54

In addition, the waveguide crossing can be applicable by combining point and linear defects [44]. As seen in the Fig 4.13, which is redrawn by the proposed FDTD method-based simulation code, two waveguides cross at the center of the PhC. The application aims to eliminate the cross-talk between channels. It is based on the tunneling between the minor point defects. The symmetry of around channels results in the orthogonality of each waveguide channel.
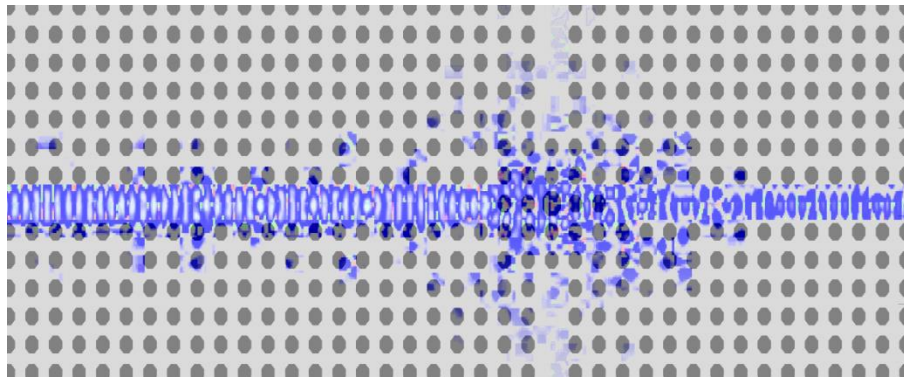

Figure 4.13. Waveguide Crossings [44]

A channel drop filter is another application [45]. As in the Fig 4.14, which is redrawn by the proposed FDTD method-based simulation code, two parallel waveguides are coupled with point defects. The point defects are in monopole states. The combination of even and odd states is coupled through the center. Therefore, each side has the same polarity but with the opposite sign. Then, the cancellation of the two coupling occurs with resulting in an exact wavelength transmission.
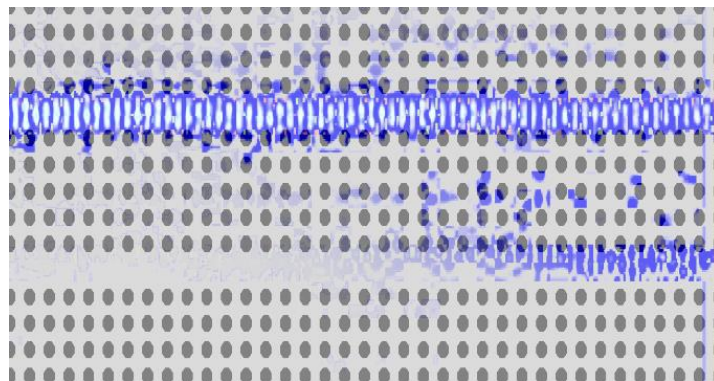

Figure 4.14. Channel-Drop Filter [45]

4.3. The Experimental Model of L3 Coupled Cavities on 2D Photonic Crystal

Photonic crystals are devices to manipulate light in various ways. Here, To simulate the structure dynamically, 2D PhC with the three missing holes (L3) is used as in the Fig 4.15, which is redrawn by the proposed FDTD method-based simulation code, makes the structure L3 cavity. The structure is composed of a single row defect and two L3 type point defects. The structure is inside a silicon medium and the air holes. The lattice period a is 420 nm, and hole radius r is $0.29a$. The separation is L_{12} is $12a$ [8,9]. Also, the close holes are shifted a distance of $s_1 = 0.15a$ To tune the cavities at resonance frequency by having all-optical analog EIT as discussed in the introduction chapter. Also, the band diagram of the L3 cavity PhC is given in the Fig 4.16, which is redrawn by MPB.
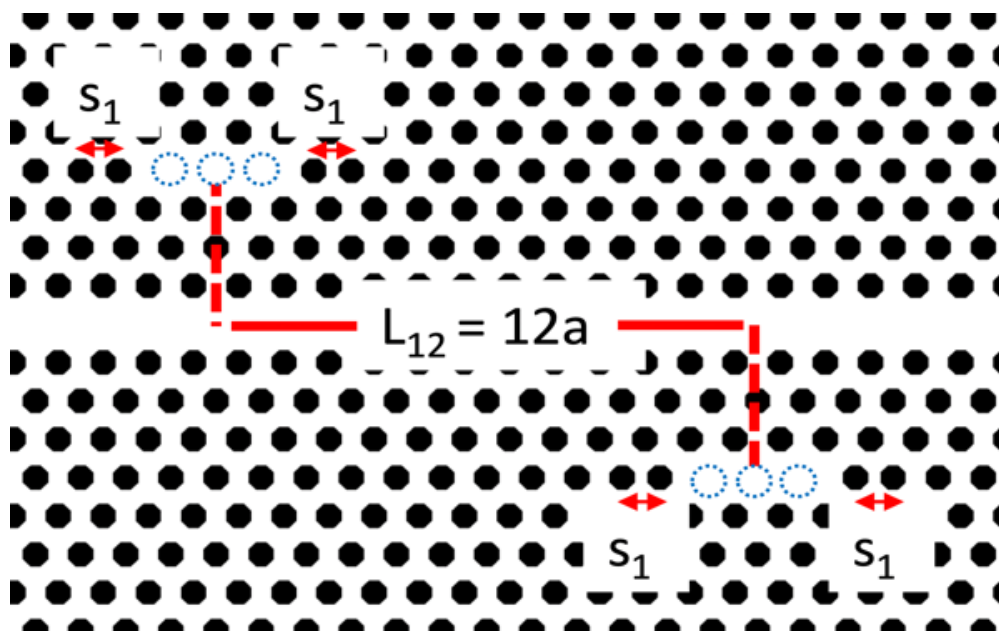

Figure 4.15. L3 Coupled Cavities PhC [8,9]

Couple mode theory states as [46],

$$\frac{da_n}{dt} = \left[-\frac{1}{2\tau_{total,n}} + i\left(w_1 + \Delta w_1 - w_{wg}\right) \right] a_n + \kappa s_{R(n-1)} \qquad (4.27)$$

At which, the total loss rate is,

$$\frac{1}{\tau_{total}} = \frac{1}{\tau_v} + \frac{1}{\tau_{in}} \qquad (4.28)$$

So, cavity-waveguide coupling is defined as [8],

$$\kappa = i \frac{e^{-\frac{i\phi}{2}}}{\sqrt{2\tau_{in}}} \qquad (4.29)$$
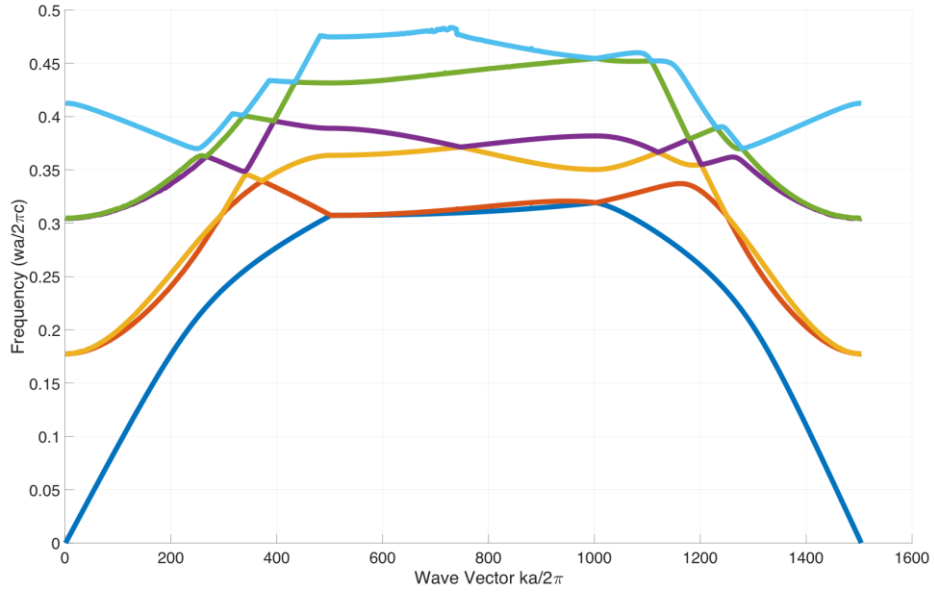

Figure 4.16. L3 Cavity PhC Band Diagram

The cavity resonances are arranged enough to have a trip phase equals to Fabry-Perrot resonances. The tune of the cavities equals to mismatch of the cavity resonances as,

$$\delta_{12} = 2(w_1 - w_2)\tau_{total} \qquad (4.30)$$

4.4. The Verification of The Proposed Method With Simulation of L3 Coupled Cavity PhC

The structure is then simulated by both MEEP and the propose dynamic FDTD. The Fig 4.16 gives the results of the MEEP, with the EIT case. Around 1550 nm, the EIT case occurs and transmission peak at the deep can be observed. At that point, the wavelength resonances are 1557.9 nm and 1561.4 nm as indicated in the experimental procedure. At this point the calculated detuning δ_{12} equals to 3.34. The comparative results with the proposed dynamic FDTD is given in the Fig 4.17, 4.18, 4.19 and 4.20.

Figure 4.17. L3 Cavity PhC simulated by MEEP
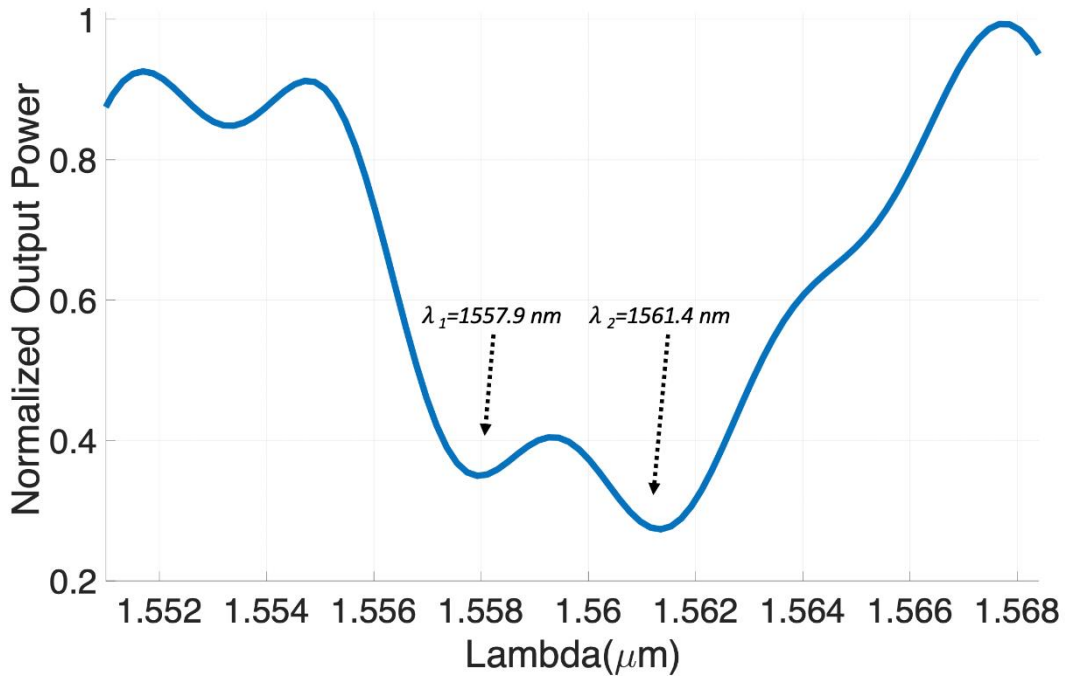
The spectral analyses of the L3 cavity PhC is given in the Fig 4.17. It can be observed that the cavity regions have illumination. This means that the EIT case occurs depending on the wavelength resonances of cavities. Around the cavities, the light is trapped, and propagation is continuing. Therefore, the light storage can be mentioned during the lifetime of the cavity, 4.15ps

The transmission belonging to the EIT case is given in the Fig 4.18. The all-optical to analog EIT case occurs at 1550nm. In this Fig, the left cavity resonance and the right cavity resonance are indicated. These points are combined with the EIT case. At the point, the peak at deep can be observed.
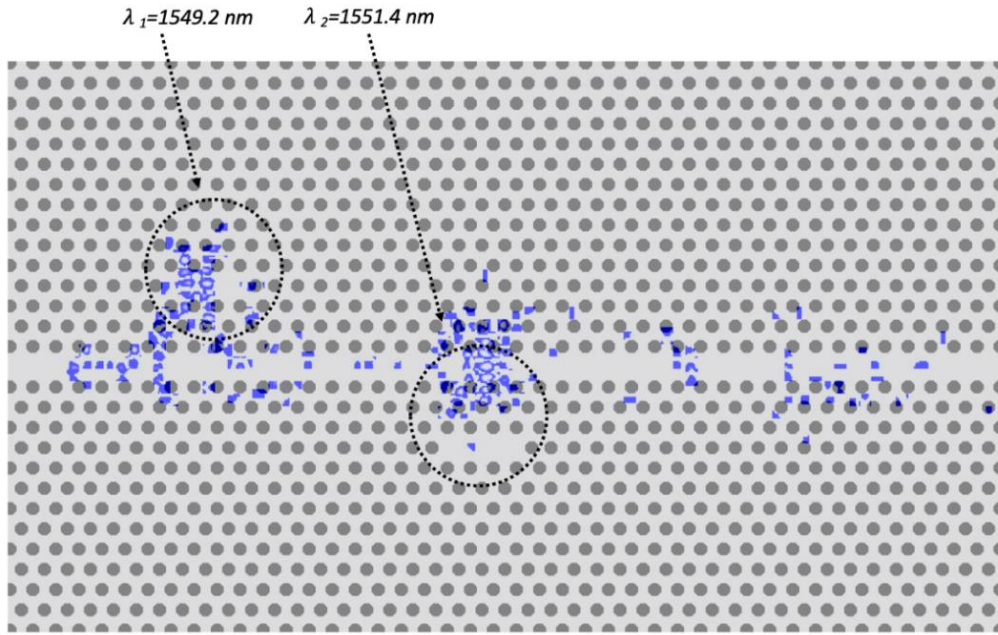

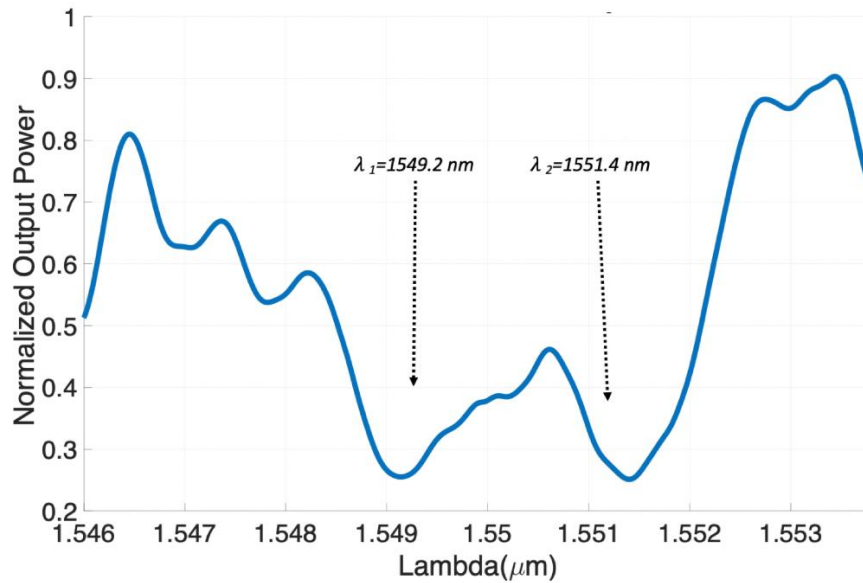
Figure 4.18. Spectrum Analyze of L3 Cavity PhC

Figure 4.19. The EIT Case of L3 Cavity PhC

The resonance wavelength difference is 1.2 nm. This results in a detuning as 3.34 which is nearly the same as the results in MEEP and experiments. Beyond single EIT case, giving an L3 cavity with a distance of $L_{23} = 30a$ results in double EIT peaks. The structure giving the result of a multi EIT case is shown in the Fig 4.19. So, the related transmission is given in the Fig 4.20. Regarding the transmission results in the Fig 4.20, the multi EIT peaks occur at the resonance wavelengths, obtained by the proposed method, $\lambda_1 = 1549.6\ nm, \lambda_2 = 1550.3\ nm$ and $\lambda_3 = 1551.1\ nm$. These give the detuning between the L3 cavities as $\delta_{12} = \delta_{23} = 0.82$.
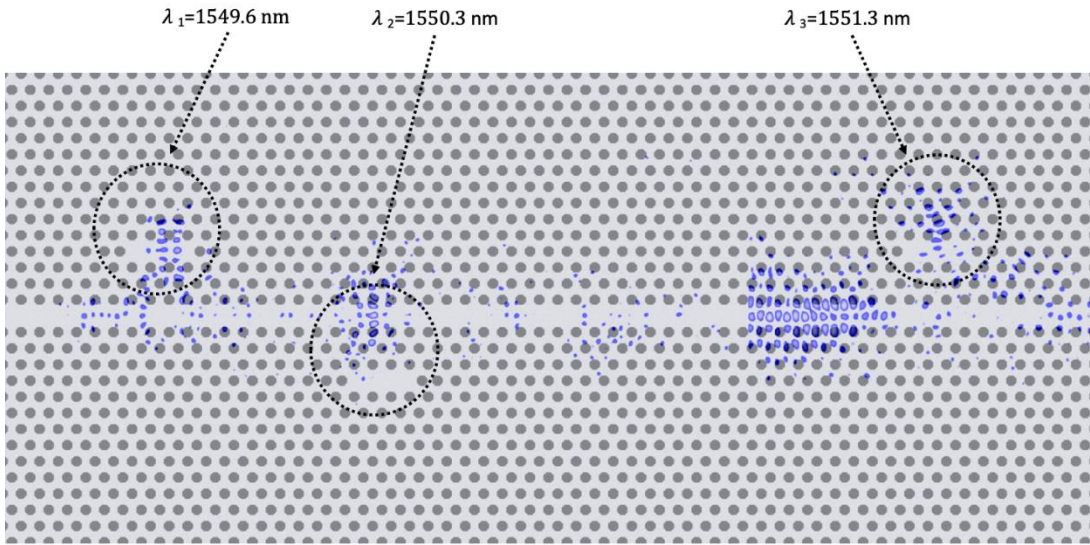
Figure 4.20. The Structure of Multi EIT case

The delay on the light which is trapped inside cavities is also simulated. Using the proposed dynamic FDTD method, the various delay times are obtained. The Figs 4.22 and 4.23 are the time-delayed light signals depending on various detuning. The Fig 4.21 is the usual light propagation. The comparative results give the delayed times as 9.62 ps and 17.2 ps. These results are the proof of the stability of dynamic FDTD simulation since the numbers are nearly identical with experimental values as the wavelength resonances for single EIT case, 1548.63 nm and 1549.45 nm and for multi EIT case, 1533.52, 1533.98 and 1534.02 [8, 9]. The proposed dynamic FDTD can be verified with comparative results with MEEP and the experiment. By comparing these

results, the proposed method gives similar wavelength resonances and detuning. Therefore, the proposed method can be used for both conventional FDTD simulation and dynamic ones. The dynamic changes, the shift in the neighbor holes, cause of the light trapping inside cavities depending on the wavelength resonances.
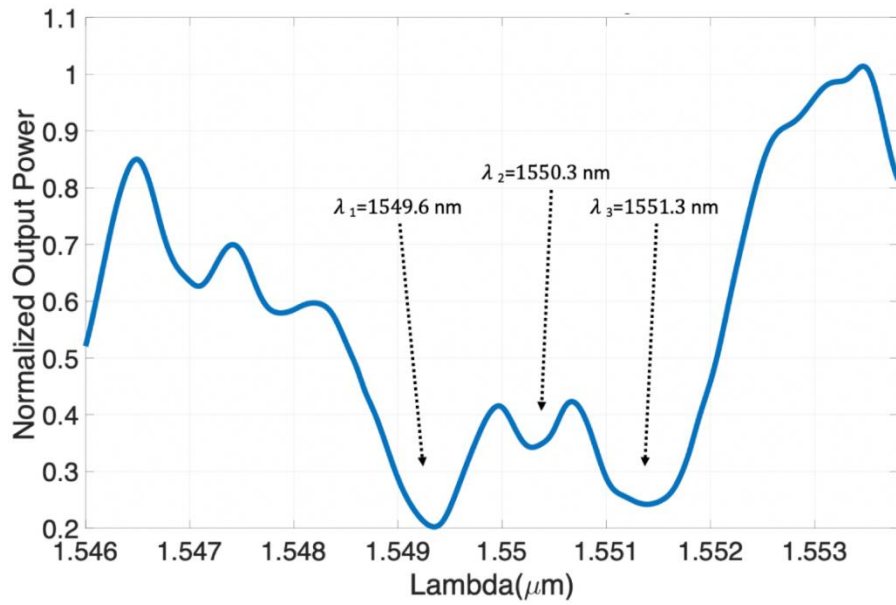

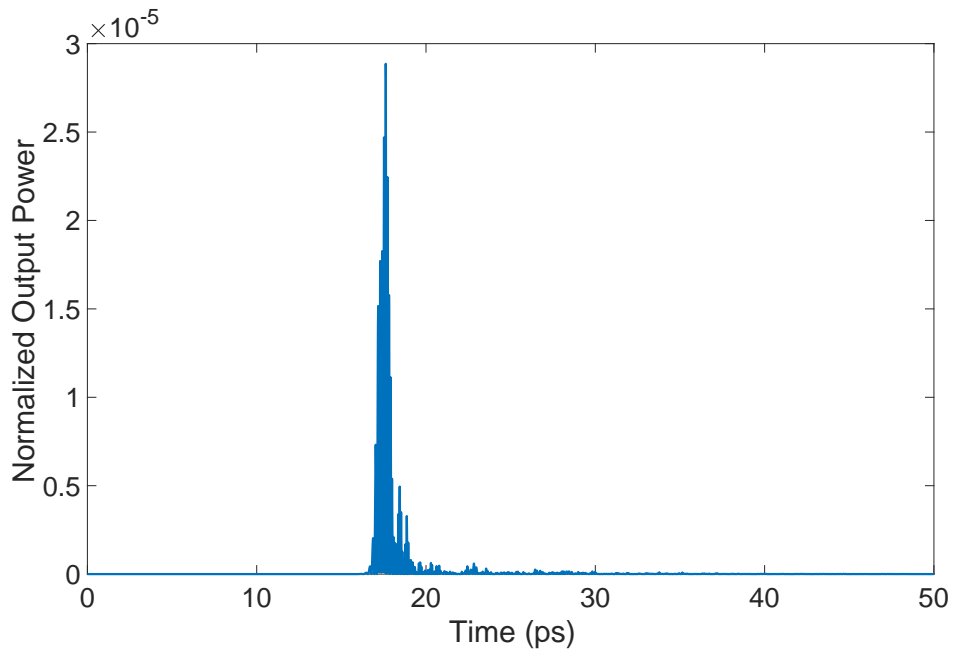*Figure 4.21. The Multi-EIT Case of L3 Cavity PhC*

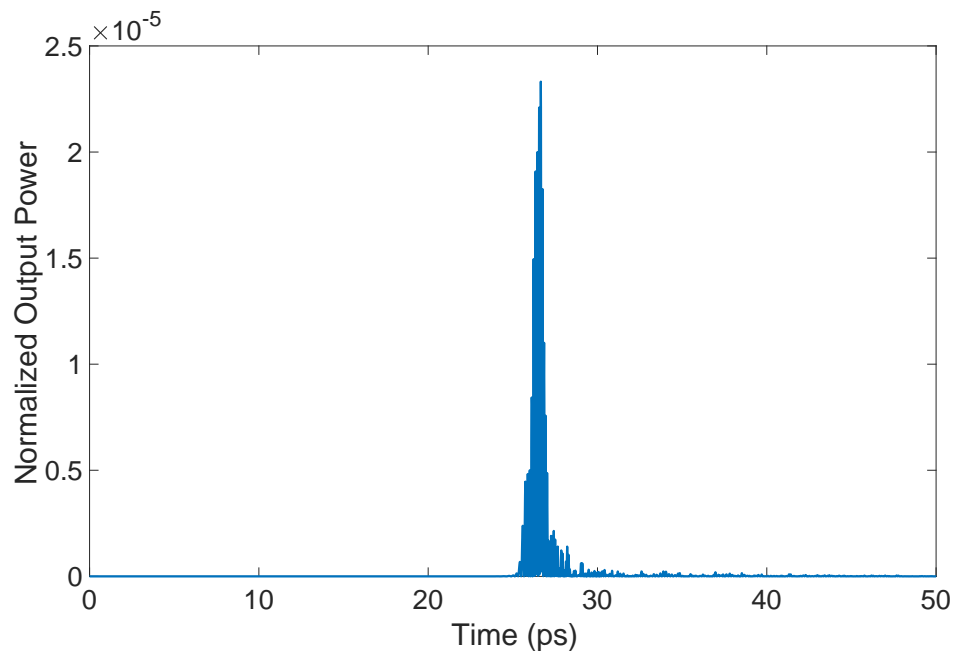*Figure 4.22 Time Scale Pulse Propagation of the non-EIT case*

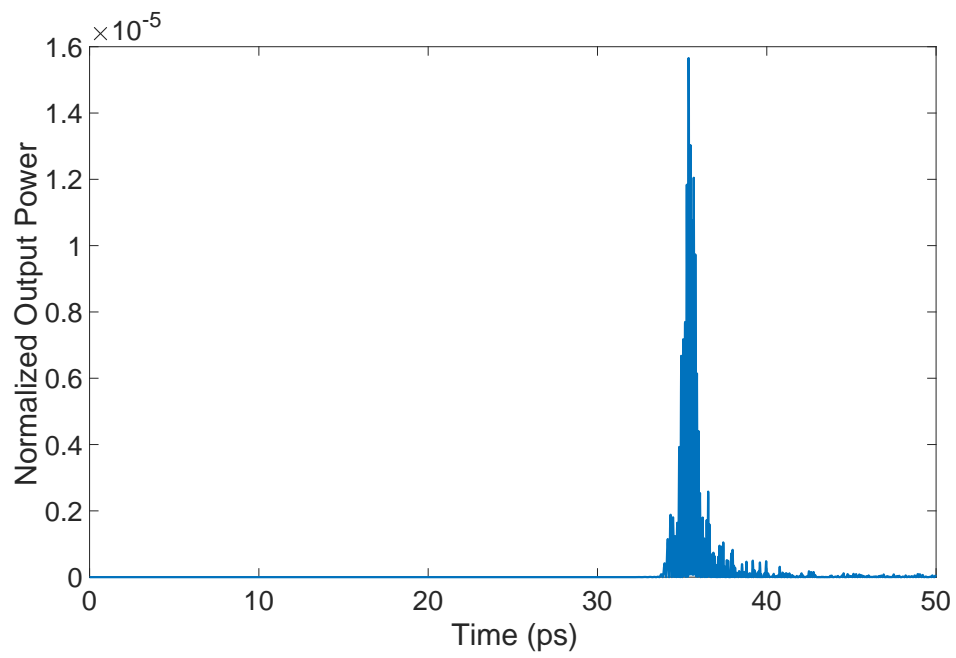*Figure 4.23 Time Scale Pulse Propagation with a Delay of 9.62ps*

Figure 4.24 Time Scale Pulse Propagation with a Delay of 17.2ps

CHAPTER 5

CONCLUSIONS AND DISCUSSIONS

In this thesis, the improved EM waves' computational analysis is demonstrated. After the literature survey about the computational analysis of the optical devices, it is inferred that for dynamical devices, there is a need for simulation tools. Beginning of that idea and considering the flexibility of the FDTD method, the improvements related to dynamical tunings are held. Before the dynamical implementation, the basis of the FDTD method an also EM theory are studied.

Each equation from Maxwell's laws are theoretically inferred. These laws are cause and consequence of the EM waves. Therefore, each EM field can be interpreted from the other. With the help of this idea, the iteration form of the FDTD method is used to calculate future values from the former fields.

Since the computational world needs discretization, all Equations of Maxwell's set are converted into discrete forms. Beginning with the Taylor series expansion, the derivative form of Maxwell's equations is approximated. Therefore, the resulted equations can be available to use for the computational world. Also, it is showed that the coefficients of the FDTD method provide stability of EM fields. These coefficients are grouped as the number called Courant Number. So, its limitation is physically given as the maximum energy per spatial grid size. To maximize this ratio, Courant Number is chosen as a maximum value of the ratio, 1. Higher values of the ratio causes of instability of the EM waves on iterative formulas.

Besides inferring to iterate EM waves, the FDTD method could be rearranged depending on experimental conditions. Therefore, the TFSF boundary is stated to have source field propagating in the right-hand direction. By interference of the scattered field with added source field, the undesired vector is eliminated.

Absorbing boundary conditions (ABC) are stated to avoid the infinite propagation of the EM fields. For the 1D FDTD method, this condition is satisfied with the equality of the first and last grid sizes. Another issue about FDTD is source implementation. The source is propagating with the displacement vector in Maxwell's equations. Then, the source is given inside the iterative form of the electric field.

The introduction to the ring resonators is examined after the implementation of the FDTD method. The various types of resonators with their applications are given. Lastly, the double ring resonator is stated. Since there are dynamical experiments that are achieved, the double ring resonator is simulated to develop dynamical FDTD. Giving the basis of the coupling theory of the double ring resonator, the FDTD method is improved.

The verification of the C++ coded FDTD method is achieved with the conventional FDTD simulation tool, MEEP is used. They compared results of MEEP and the proposed dynamic FDTD are given with stationary double ring resonator. The EIT and open states are simulated individually with both MEEP and the dynamic FDTD. The results of these two tools are similar. Therefore, the proposed dynamic FDTD is taken as the verified method for simulating both static and dynamic cases, individually. For the static case, the effective refractive indexes of rings are identical which gives the non-EIT results. The dynamic case states the 0.35 nm wavelength difference between the effective refractive index of the rings corresponding to the EIT case. These cases are simulated individually by both MEEP and the proposed FDTD method.

For dynamical tuning of the double microring resonator, the EIT cases depending on the refractive index change that creates wavelength difference between the ring waveguides are illustrated. This illustration is achieved by tuning during the simulation run. The instant change in the refractive index during simulation gives the results concerning the EIT case. By using the spatial distribution of the EM waves inside the resonator, the tune-detune states are demonstrated. After that, the dynamic results that are based on the instant refractive index change, are given with delaying light. The increase in the tuning results in a more extended storage of light inside the resonator. Therefore, the consistent storage times state that the proposed dynamic FDTD works well. After the double microring resonator, the L3 cavity PhC is also dynamically simulated. By shifting the neighbor holes, the EIT case is created. As discussed in the introduction chapter, using the difference between the wavelength resonances, the light is trapped inside the resonator. Also, the multi EIT case is simulated by imposing an extra L3 cavity. Then, the multiple EIT peaks are observed. Also, using the proposed dynamic FDTD, the light is delayed with a proportion of the storage times. This means by controlling the tuneability, the light can be stored at a desired time. All these simulations give consistent results with both MEEP and experimental works [6, 7, 8, 9]. Since the comparative results verify the propose dynamic FDTD results, the method is useful for both static and non-stationary objects which have difference in refractive index dynamically..

The simulations of both double microring resonator and L3 coupled cavity PhC are taken as two dimensional. Therefore, the exact verification of the proposed method would take consider the third dimension to compare simulation results with the experimental works [6, 7, 8, 9]. The improvement of the proposed method needs to consider the z-axis along the structure.

The proposed dynamic FDTD method is used for a double microring resonator with the alteration of the refractive index. However, there are optical devices such that photonic crystals, Mach Zehnder interferometers or other types of ring resonators. Therefore, the proposed method can be arranged to simulate such devices. The

65

flexibility of the FDTD method makes this thought available. Moreover, in this work, the method is represented for the refractive index change. From the literature survey, it is also used for moving PhC. Therefore, dynamic tunes can be widening in other properties. Temperature change, size change would be the next step for the proposed method. Therefore, the C++ coded dynamic FDTD method can be expanded to optical devices with various conditions.

REFERENCES

[1] Bigelow, M. S., Lepeshkin, N. N. & Boyd, R. W. "Superluminal and slow light propagation in a room-temperature solid". Science 301, 200–202 (2003).

[2] Hau, L. V., Harris, S. E., Dutton, Z. & Behroozi, C. H." Light speed reduction to 17 meters per second in an ultracold atomic gas". Nature 397, 594–598 (1999).

[3] Ghosh, S., Sharping, J. E., Ouzounov, D. G. & Gaeta, A. L. "Resonant optical interactions with molecules confined in photonic band-gap fibers". Phys. Rev. Lett. 94, 093902 (2005).

[4] Liu, C., Dutton, Z., Behroozi, C. H. & Hau, L. V. "Observation of coherent optical information storage in an atomic medium using halted light pulses". Nature 409, 490–493 (2001).

[5] Phillips, D. F., Fleischhauer, A., Mair, A., Walsworth, R. L. & Lukin, M. D. "Storage of light in atomic vapor". Phys. Rev. Lett. 86, 783–786 (2001).

[6] Xu Q. et al., "Experimental Realization of an On-Chip All- Optical Analogue to Electromagnetically Induced Transparency". Physical Review Letters PRL 96, 123901(2006)

[7] Xu Q, Dong P. and Lipson M.," Breaking the Delay-Bandwidth Limit in a Photonics Structure". Nature Physics Vol 3 (2007)

[8] Kocaman, S., et. al, "Observations of Temporal Group Delays in Slow-Light Multiple Coupled Photonic Crystal Cavities." Applied Physics Letters 96, no. 22 (2010)

[9] Yang X., et al, "All-Optical Analogue to Electromagnetically Induced Transparency in Multiple Coupled Photonic Crystal Cavities" Physical Review Letters, 1002i 173902 (2009)

[10] Soref R. A. and Bennett B. R. "Electrooptical Effects in Silicon". IEEE Journal of Quantum Electronics Vol. QE-23 No.1 (1987)

[11] Joannopoulos J. D., Johnson S. G. Winn J. N. and Meade R. D., Photonic Crystals Molding the Flow of Light, Princeton University Press, second edition 190-199, 2008

[12] Pollock C. R. and Lipson M., Integrated Photonics, Springer Science Business Media, LLC first edition 233-237, 2003

[13] Bogaerts W. Et al, "Silicon Microring Resonators", Last Photonics Rev. 6 No.1, 47-73(2012)/DOI 10.1002/lpor.201100017 (2011)

[14] Harris S. E. "Electromagnetically Induced Transparency", Physics Today 50:36 doi:10.1063/1.881806 (1997)

[15] Marangos J. P. "Electromagnetically Induced Transparency" Journal of Modern Optics, Vol. 45 No. 3 471-503 (1998)

[16] Peng B et al, "What is and what is not electromagnetically induced transparency in whispering-gallery microcavities". Nature Communications Vol. 5 (2014)

[17] Schneider J. B, Understanding the Finite Difference Time Domain Method, April 5,2016

[18] Inan U. S. and Marshall R. A., Numerical Electromagnetics The FDTD Method, Cambridge University Press, first edition, 342-383, 2011

[19] Kane S. Yee, "Numerical Solution of Initial Boundary Value Problems Involving Maxwell's Equations in Isotropic Media". IEEE Transactions on Antennas and Propagation Vol. Ap-14   No.3 (1966)

[20] Hafner C, The Generalized Multipole Technique Computational Electromagnetics, Artech House Publishers, pp 157-212, (1990)

[21] Hafner C., "Multiple Multipole Program Computation of Periodic Structure", J. Opt. Soc. Am. Vol. 12 No.5, (1995)

[22] Busch K., Blum C., Graham A. M., et al," The Photonic Wannier Function Approach to Photonic Crystal Simulations: Status and Perspectives", J. Mod. Opt. Vol.58, Nos. 5-6, (2011).

[23] Blum C., Wolff C., and Busch K., "Photonic-Crystal Time-Domain Simulations Using Wannier Functions", Opt. Lett. Vol.36, no.2 (2011).

[24] Li L, "Formulation and Comparison of Two Recursive Matrix Algorithms for Modeling Layered Diffraction Gratings", J. Opt. Soc. Am. A Vol. 13, No.5 (1996).

[25] Li L., "New Formulation of the Fourier Modal Method for Crossed Surface-Relief gratings", J. Opt. Soc. Am. A Vol. 14, No.10 (1997).

[26] Essig S. and Busch K., "Generation of Adaptive Coordinates and their Use in The Fourier Modal Method", Opt. Express Vol.18, No.22 23258 (2010).

[27] Shankar V. and Hall W.F. "A Time Domain Differential Solver for Electromagnetic Scattering", in URSI National Meeting, Boulder, CO, 1988

[28] Madsen N. K. and Salkowski R. W., "Numerical Solutions of Maxwell's Equations in The Time Domain Using Irregular Nonorthogonal Grids", Waves Motion, vol. 10, pp 530-590, 1988

[29] Taflove A. and Hagness S. C., Computational Electrodynamics the Finite Difference Time Domain Method, Artech House third edition 51-105, 2005

[30] Hesthaven J. S., Gottlieb S. and Gottlieb D., Spectral Methods for Time-Dependent Problems, Cambridge University Press, 2007

[31] Jin J., The Finite Element Method in Electromagnetics, John Wiley & Sons, New York, third edition, pp 513-628, 2014

[32] Pelosi G., "The Finite-Element Method, part i: R. I. Courant", IEEE antennas and Propagation magazine, vol. 49, pp. 180-182 (2007)

[33] Busch K., König M. and Niegemann J. "Discontinuous Galerkin Methods in Nanophotonics", Laser Photonics Review, Rev. 5, No. 6, 773‑809 / DOI 10.1002/lpor.201000045, (2011)

[34] Niegemann J, Pernice W and Busch K, "Simulation of Optical Resonators Using DGTD and FDTD", Journal of Optics, 11 (2009)

[35] Jiang Q. et al., "Mechanism Analysis of the Inverse Doppler effect in Two-Dimensional Photonic Crystal based on Phase Evolution". Scientific Reports 6:24790 DOI:10.1038/srep24790 (2016)

[36] Saleh E. A. and Teich M. C., Fundamental of Photonics, John Wiley & Sons, second edition, pp-160-209, 2007

[37] Rao S. M., Time Domain Electromagnetics, Academic Press, first edition, pp 151-237, 1999

[38] Heebner J., R. Grover, and Ibrahim T., Optical Microresonators: Theory, Fabrication and Applications, 1st edition., Springer Series in Optical Sciences (2008)

[39] Heebner J., Wong V., Schweinsberg A., et al, IEEE J. Quantum Electron. 40(6), 726–730 (2004).

[40] Katti R. and Prince S," Analysis of Serial and Parallel Cascaded Microring Resonators: An FDTD Approach", Optik Vol. 152 (2018)

[41] Mayonado G., Mian S. M., Robbiano V and Cacialli F, "Investigation the Bragg-Snell Law in Photonic Crystal", American Association of Physics, (2015)

[42] Armstrong E. and O'Dwyer C., "Artificial Opal Photonic Crystals and Inverse Opal Structures-Fundamentals and Applications from Optics to Energy Storage", Journal of Material Chemistry, Vol. 3, (2015)

[43] Kwon S., Kamp M. et al, "Elimination of Cross-Talk in Waveguide Intersections of Triangular Lattice Photonic Crystals", Optics Express, Vol. 16, No. 15, (2008)

[44] Johnson S. G., Manolatou C. et al, "Elimination of Cross Talk in Waveguide Intersections", Optics Letters, Vol. 23, No.23, (1998)

[45] Fan S., Villeneuve R. and Joannopoulos J. D.,” Channel Drop Tunneling Through Localized States, Physical Review Letters”, Vol. 80, No.5, (1998)

[46] Haus H. A., Waves and Fields in Optoelectronics, Prentice-Hall, Englewood Cliffs, chap. 7 p. 197, 1984

[47] Fleischhauer M, Imamoglu A. and Marangos J. A. “Electromagnetically Induced Transparency: Optics in Coherent Media” (2004)

[48] Harris S. E., “Lasers without Inversion: Interference of Lifetime-Broadened Resonances”, Phys. Rev. Lett. Vol. 62, (1989)

[49] Hafner C. and Bomholt L. H., The 3D Electrodynamic Wave Simulator, 1993

[50] Farjadpour A., Roundy D. et al,” Improving Accuracy by Subpixel Smoothing in The Finite-Difference Time Domain”, Optics Letters, Vol. 31, No.20, (2006)

[51] Deinega A. and Valuev I., “Subpixel Smoothing for Conductive and Dispersive Media in The Finite-Difference Time-Domain Method”, Optics Letters, Vol. 32, No.23, (2007)

[52] Oskooi A. F., Kottke C. and Johnson S. G., “Accurate Finite-Difference Time-Domain Simulation of Anisotropic Media by Subpixel Smoothing”, Optics Letters, Vol.34, No.18, (2009)

[53] Azar C. L. G., Martinez M. A. G. and Nussenzveig P., “Classical Analog of Electromagnetically Induced Transparency”, Am. J. Physics Vol 70. (2002).